







RESEARCH ARTICLE

Correlating deformation events onshore and offshore in superimposed rift basins: The Lossiemouth Fault Zone, Inner Moray Firth Basin, Scotland

Alexandra Tamas^{1,2}  | Robert E. Holdsworth^{1,3}  | John R. Underhill^{4,5} |
Dan M. Tamas²  | Edward D. Dempsey⁶  | Dave J. McCarthy⁷  |
Ken J. W. McCaffrey^{1,3}  | David Selby^{1,8}

¹Department of Earth Sciences,
Durham University, Durham, UK

²Department of Geology and Centre
for Integrated Geological Studies,
Babes-Bolyai University, Cluj-Napoca,
Romania

³Geospatial Research Ltd, Durham, UK

⁴Shell Centre for Exploration
Geoscience, Institute of GeoEnergy
Engineering, Heriot-Watt University,
Edinburgh, UK

⁵Centre for Energy Transition, School of
Geosciences, King's College, Aberdeen,
UK

⁶Department of Geology, Hull
University, Hull, UK

⁷British Geological Survey, Edinburgh,
UK

⁸State Key Laboratory of Geological
Processes and Mineral Resources,
School of Earth Resources, China
University of Geosciences, Wuhan,
Hubei Province, China

Correspondence

Alexandra Tamas, Department of Earth
Sciences, Durham University, Durham,
UK.

Email: alexandra.tamas@durham.ac.uk

Funding information

British Geological Survey; Durham
University; Natural Environment
Research Council

Abstract

The separation and characterisation of different deformation events in superimposed basins can be challenging due to the effects of overprinting and/or fault reactivation, combined with a lack of detailed geological or geophysical data. This paper shows how an onshore study can be enhanced using a targeted interpretation of contiguous structures offshore imaged by seismic reflection data. Two deformation events, including evidence of fault reactivation, are recognised and associated with the onshore part of the Lossiemouth Fault Zone (LFZ), southern-central Inner Moray Firth Basin. The basin is thought to record a history of Permian to Cenozoic deformation, but it is difficult to conclusively define the age of faulting and fault reactivation. However, structures in onshore outcrops of Permo–Triassic strata show no evidence of fault growth, and new interpretation of seismic reflection profiles in the offshore area reveals that Permo–Triassic fills are widely characterised by subsidence and passive infill of post-Variscan palaeotopography. We propose that sequences of reactivated faulting observed onshore and offshore can be correlated and can be shown in the latter domain to be Early Jurassic–Late Cretaceous, followed by localised Cenozoic reactivation. The workflow used here can be applied to characterise deformation events in other superimposed rift basins with contiguous onshore (surface)—offshore (subsurface) expressions.

KEYWORDS

fault reactivation, Inner Moray Firth Basin, North Sea, superimposed deformation

This is an open access article under the terms of the [Creative Commons Attribution](https://creativecommons.org/licenses/by/4.0/) License, which permits use, distribution and reproduction in any medium, provided the original work is properly cited.

© 2022 The Authors. *Basin Research* published by International Association of Sedimentologists and European Association of Geoscientists and Engineers and John Wiley & Sons Ltd.

1 | INTRODUCTION

Superimposed sedimentary basins are vertically stacked basins that partially or completely overlap. These types of basins are very common. Examples include the Colorado basin (Lovecchio et al., 2018); East African Rift (Macgregor, 2015; Ragon et al., 2018); Gulf of Aden (Fournier et al., 2004); Northeast Atlantic margin (Hansen et al., 2012; Henstra et al., 2019); East Greenland rift system (Rotevatn et al., 2018); Northwest shelf of Australia (Deng & McClay, 2021; Deng et al., 2020, 2021); Black Sea (Bosworth & Tari, 2021); North Sea rift (e.g., Tomasso et al., 2008) and West Orkney Basin (Wilson et al., 2010). In such superimposed basins, isolating and characterising the age and structural styles associated with individual deformation events is commonly difficult to constrain. This may be due to insufficient or ambiguous geological or geophysical data (e.g., poor seismic resolution), which can lead to uncertainties or contrasting models regarding the age and kinematics of fault motion and/or fault reactivation. Onshore areas may be limited by poor surface exposure and lack of constraints concerning the absolute/relative age of fault movements. A better understanding of the timing of deformation can provide key insights into basin development and potentially reduce subsurface uncertainties. It allows key rift-related faulting and inversion events to be more accurately related to the basin burial and uplift history, which leads in turn to an improved prediction of hydrocarbon development and entrapment processes. For example, Tamas et al. (2021) have shown how geochronological dating of syn-tectonic calcite mineral fills associated with basin-related faults exposed onshore can be used to better constrain the age of faulting episodes in the offshore area of the Inner Moray Firth Basin, Scotland. In this paper, we use an example from the same basin in an onshore area where calcite mineralisation is absent to show how an alternative but complementary approach can be used to the same ends. An integrated interpretation of contiguous structures seen in offshore seismic data and onshore outcrops is used to shed further light on the nature, age and significance of regional deformation events.

2 | GEOLOGICAL OVERVIEW

2.1 | Regional structural framework

The Inner Moray Firth Basin (IMFB) is a superimposed rift basin developed on Precambrian to Caledonian metamorphic basement and Devonian–Carboniferous sedimentary rocks related to the older and much larger Orcadian Basin (Figure 1; Tamas et al., 2021 and references therein).

Highlights

- Passive infill and onlaps on a pre-existing topography are observed during Permo-Triassic.
- Evidence of fault reactivation, onshore and offshore, is provided.
- Oblique-slip kinematics are recognised in both outcrops and reflection seismic data.

From the Permian to the Late Cretaceous, it formed the western part of the intra-continental North Sea trilete rift system (Andrews et al., 1990; Frostick et al., 1988; McQuillin et al., 1982; Roberts et al., 1990; Thomson & Underhill, 1993; Underhill, 1991). The rift basin is controlled by major basin-bounding faults including the Banff Fault to the south, the Helmsdale and Great Glen faults to the northwest and the Wick Fault to the north (Figure 1b). The IMFB transitions eastwards into the Outer Moray Firth basin, linking with the Central and Viking graben in the central part of the North Sea (Figure 1a). The IMFB is known to record important episodes of Late Cretaceous–Cenozoic regional uplift and faulting, including strike-slip reactivation of major basin-bounding structures such as the Great Glen (dextral) and Helmsdale (sinistral) faults (e.g., Le Breton et al., 2013; Thomson & Underhill, 1993; Underhill, 1991).

The geological history of the IMFB has, however, been a source of controversy. In particular, the Permo–Triassic history—which is widely characterised by active rifting in other parts of the North Sea (e.g., Bell et al., 2014; Fazlikhani et al., 2020; Steel & Ryseth, 1990)—is debatable in the IMFB. Some authors have considered the Permo–Triassic history to be characterised by active rifting (e.g., Frostick et al., 1988; Roberts et al., 1989). Others, based on interpretations of increasingly available seismic reflection data, considered that the Permo–Triassic history was dominated by thermal subsidence (Andrews et al., 1990; Thomson & Underhill, 1993).

During Late Jurassic–Early Cretaceous basin development, Roberts et al. (1990) and other authors (e.g., Bird et al., 1987; McQuillin et al., 1982) favoured a transtensional origin for the IMFB. Such models suggested that the basin opened due to dextral movements along the Great Glen Fault during NE–SW extension.

Underhill (1991) challenged the transtensional model, suggesting that after a long period of thermal subsidence during Triassic to Mid-Jurassic, the IMFB developed mainly during the Late Jurassic under a NW–SE to NNW–SSE orthogonal extensional regime. The majority of this extension has been interpreted to occur along the Helmsdale Fault, with synkinematic sequence thickening

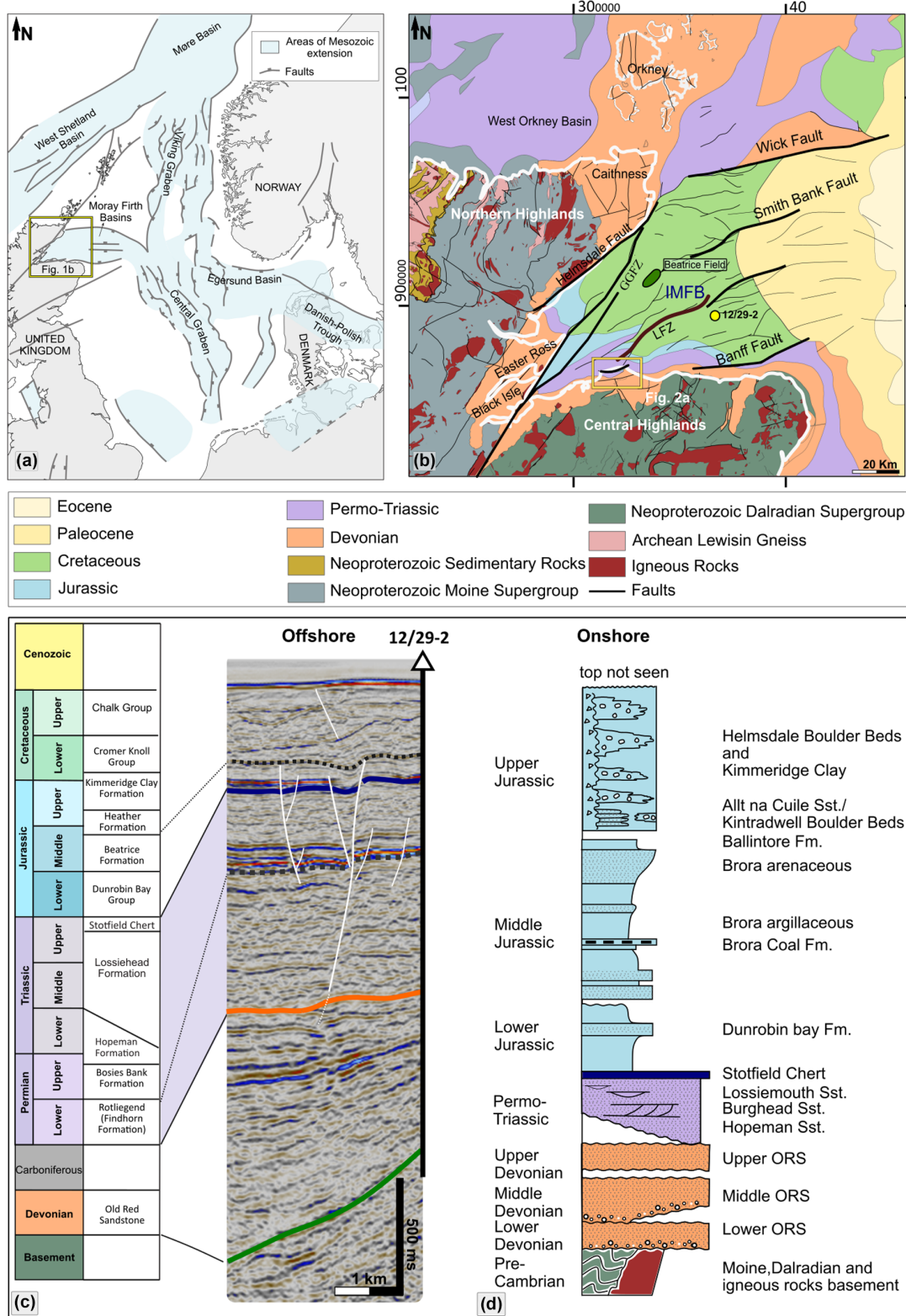


FIGURE 1 (a) Generalised tectonic map of northwest Europe showing the main Mesozoic rift systems (adapted after Goldsmith et al., 2003). Yellow box shows location of map in (b). (b) Regional geological map of northern Scotland and associated offshore regions (after Tamas et al., 2021). Yellow box shows location of Figure 3a—the onshore study area. IMFB—Inner Moray Firth Basin. LFZ—Lossiemouth Fault Zone. GGFZ—Great Glen Fault Zone. (c) Simplified offshore lithostratigraphic units of the IMFB (compiled after Andrews et al., 1990; Glennie et al., 2003). A representative section of seismic reflection data from a 2D survey is shown to illustrate (parts of) the typical seismic stratigraphy in the area. Formation tops are calibrated with the information in well 12/29-2, which crosses this seismic section (see well location on b). (d) Onshore IMFB stratigraphy (modified after Trewin & Hurst, 2009). Not to scale, with relative thicknesses shown being notional. ORS, Old Red Sandstone

observed towards the Helmsdale Fault, but not across the Great Glen Fault. This indicates that the Great Glen Fault was inactive during the Late Jurassic.

Most recent studies of offshore 3D seismic reflection profiles (e.g., Davies et al., 2001; Long & Imber, 2010; Lăpădat et al., 2016) have argued for a predominance of orthogonal rifting and suggest there is little evidence of oblique-slip faulting in the basin. However, Tamas et al. (2021) provide field evidence that strike-slip and oblique-slip faults are recognised in the IMFB basin during basin development, notably along NNE–SSW and NW–SE trends. These faults are thought to represent reactivated Palaeozoic structures related to the earlier Orcadian Basin, which were obliquely reactivated during NW–SE opening of the IMFB. The scale of this deformation is relatively minor compared with NE–SW trending major growth faults, but it highlights that the development of the IMFB is more complex and may at least *locally* be transtensional due to structural inheritance.

Following the cessation of rifting, the IMFB experienced a period of thermal subsidence during the Late Cretaceous (Underhill, 1991). From the early Cenozoic to the present day, the basin experienced episodes of uplift, eastward tilting and regional erosion, with some major faults being reactivated (e.g., Argent et al., 2002; Underhill, 1991). The Great Glen Fault is believed to be a major controlling feature at this time (Underhill, 1991). In the offshore, seismic reflection profiles show evidence for the development of strike-slip-related deformations (e.g., flower-structures, folds) that offset post-rift reflectors (e.g., Davies et al., 2001; Thomson & Underhill, 1993; Underhill & Brodie, 1993). Cenozoic structures in the onshore area supposedly include the development of NW–SE trending large-scale folds (of about 500 m wavelength) in the hangingwall of Helmsdale Fault (Thomson & Hillis, 1995; Thomson & Underhill, 1993). In addition, minor folds and faults consistent with dextral kinematics, cropping out on Easter Ross coast (Figure 1b), are also considered to be Cenozoic and to be related to right-lateral slip along the Great Glen Fault (e.g., Le Breton et al., 2013; Underhill & Brodie, 1993). The effects of Cenozoic deformation away from the Great Glen Fault, both onshore and offshore, are less certain and may be limited and/or localised.

2.2 | Regional stratigraphic framework

The IMFB area has been a sedimentary basin since the Devonian, with up to 16 km of sedimentary rocks accumulated in its deepest parts (Andrews et al., 1990). In the offshore, the preserved stratigraphy comprises Devonian to Late Cretaceous sedimentary rocks (Figure 1b,c; see also Figure S1c). Younger, Cenozoic stratigraphy is

preserved further east in the Outer Moray Firth (Figure 1b). Onshore, the exposure is mainly represented by Devonian cover sequences, which unconformably overlie the Precambrian Moine and Dalradian basement, together with Permo–Triassic to Jurassic cover sequences of limited extent (Figure 1d).

The Devonian sequence is widely distributed both onshore and offshore (e.g., well 12/29-2, Figure 1c). The succession is dominated by non-marine, red coloured alluvial and fluvial breccio-conglomerates and conglomerates, medium- to coarse-grained sandstones or flood-plain mudstones and locally lacustrine fish-bearing flagstones (e.g., Johnstone & Mykura, 1989; Stephenson & Gould, 1995, and reference therein).

Permo–Triassic strata unconformably overlie the Devonian sequences. In the offshore region, this boundary is sometimes marked by a strong reflector referred to as the ‘Variscan unconformity’ (e.g., Underhill & Brodie, 1993). This boundary is thought to reflect the development of a basin-wide erosion surface following regional-scale Variscan deformation and uplift of northern Britain in the Late Carboniferous–Early Permian (e.g., Coward et al., 1989; Seranne, 1992; Underhill & Brodie, 1993).

In the offshore, the Permian Findhorn Formation (Rotliegend Group) is dominated by sandstones and claystones of fluvial origin and is overlain by the fluvio-lacustrine deposits of the (Zechstein Group) Bosies Bank Formation (e.g., Cameron, 1993; Glennie et al., 2003). The overlying Hopeman Formation forms a thick sequence of dune bedded aeolian sandstones (e.g., Peacock et al., 1968) considered to be topmost Permian to basal Triassic (Benton & Walker, 1985; Clemmensen, 1987; Walker, 1973). In the onshore, the Permian deposits have a restricted coastal exposure almost entirely along the southern coast of the IMFB (Figure 2a). In general, they are characterised by aeolian, dune bedded sandstones, playa deposits and conglomerates interbedded with cross-bedded sandstones, part of a marginal fluvial sequence (e.g., Stephenson & Gould, 1995).

The Triassic strata in the offshore IMFB comprise mainly fluvial, alluvial fan or lacustrine red bed sandstones and shales of the Lossiehead Formation (Goldsmith et al., 2003). On the south coast onshore, the Triassic is represented by the laterally equivalent fluvial Burghead Sandstone and younger, mainly aeolian Lossiemouth Sandstone (e.g., Frostick et al., 1988). This succession is capped by the Stotfield Chert, a ca. 25 m thick calcareous layer, locally dominated by microcrystalline silica (e.g., Frostick et al., 1988). This layer is interpreted as a palaeosol horizon formed during a phase of tectonic quiescence (Naylor et al., 1989), which is also recognised in offshore wells and seismic reflection profiles (Figure 1c).

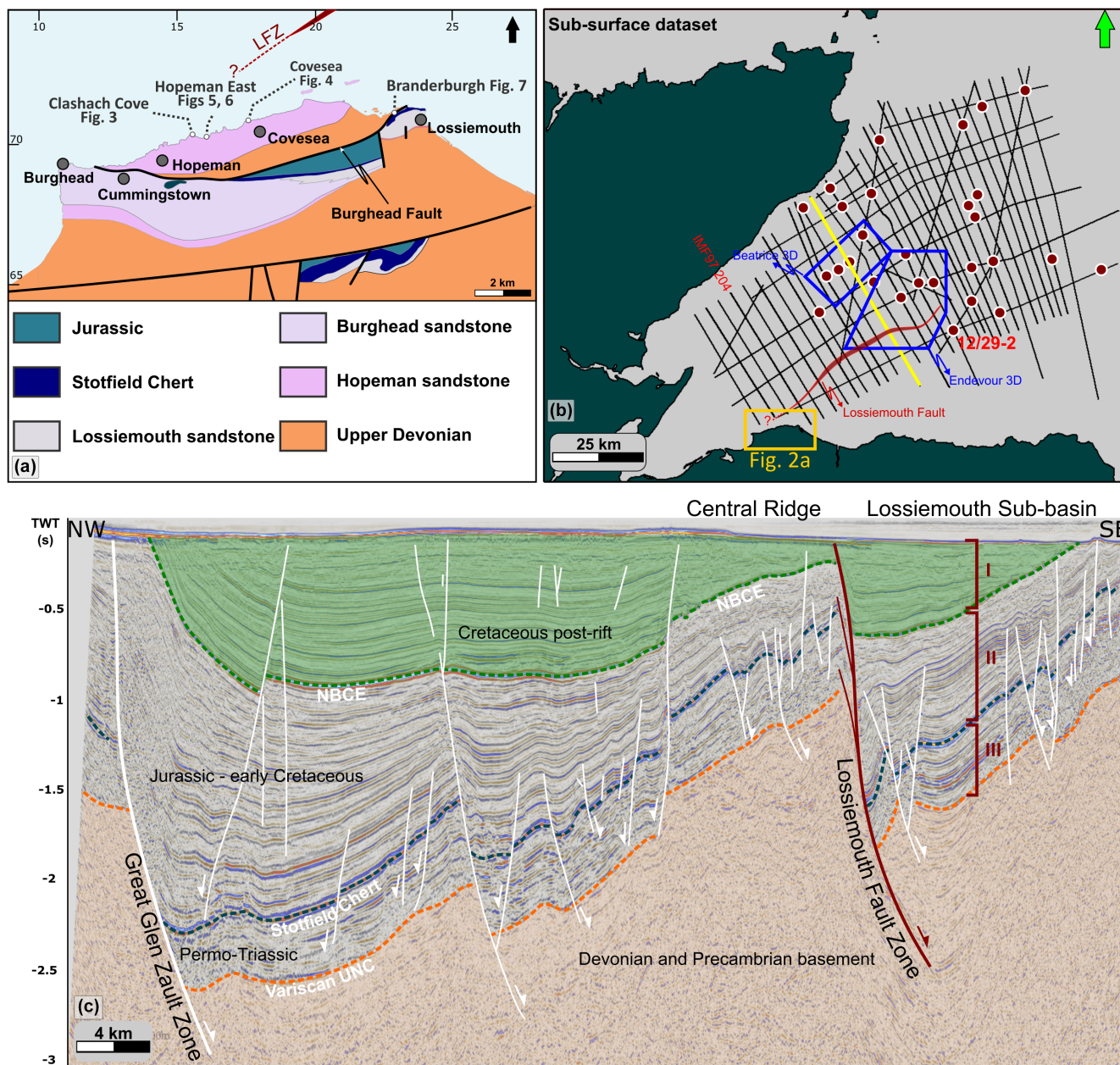


FIGURE 2 (a) Geological map of the onshore study area (modified after BGS, 1969) The locations of Figures 3–7 are also shown. (b) Map of offshore data used for this study. 2D seismic lines are shown in yellow, and 3D cubes in blue. The seismic line shown in (c) is shown in bold. The red circles represent wells. The well mentioned in Figure 1c and the text is labelled (c) Regional seismic section across the study area showing the interpreted horizons and the main faults, including the LFZ. I–III represent the investigated stratigraphic sequences referred to in the text

The overlying Lower/Middle Jurassic succession is generally represented by fluvial sandstones and shales, deltaic sandstones and coals (e.g., Linsley et al., 1980; Trewin & Hurst, 2009) which in the offshore domain belong to the Dunrobin Bay, Beatrice and Heather formations. The following Upper Jurassic Kimmeridge Clay Formation is characterised by marine shales, sandstones and locally debris flow breccias. An almost complete section of Jurassic strata, with similar facies to offshore, crops out on the

north-western coast of the IMFB. The Jurassic-Lower Cretaceous boundary is considered intra-formational, lying within the Kimmeridge Clay Formation (Rawson & Riley, 1982).

The Upper Jurassic sequences are capped by the second most prominent seismic reflector seen in the offshore IMFB, which is variously termed the ‘Base Cretaceous unconformity’ (Thomson & Hillis, 1995), ‘(Near) Base Cretaceous unconformity’ (Long & Imber, 2010) or ‘(Near)

Base Cretaceous Event' (Underhill, 1991; Underhill & Brodie, 1993). As this marker event represents both a local to regional unconformity, but also locally conformable and condensed sections are present (Rawson & Riley, 1982), we refer to it here as the Near Base Cretaceous Event (NBCE).

The Cretaceous sequence is limited to the offshore parts of the IMFB and is generally well-imaged above the NBCE seismic marker. It is characterised by onlapping reflectors, which progressively encroach onto the basin margins (e.g., Thomson & Underhill, 1993). The Lower Cretaceous sequences comprise predominantly marine sandstones and calcareous shales of the Cromer Knoll Group, followed by the Upper Cretaceous Chalk group comprising a thick sequence of coccolithic limestone, marls and glauconitic sandstones (e.g., Andrews et al., 1990). The Cenozoic sequence is restricted to the offshore Outer Moray Firth and extends eastwards to the Central and Viking grabens (Figure 1b).

2.3 | Lossiemouth Fault Zone (LFZ)

The composite sub-parallel faults forming the Lossiemouth Fault Zone (LFZ) lie on the southern side of the IMFB (Figures 1b and 2b) and are thought to extend both onshore and offshore (e.g., Al-Hinai et al., 2008; Farrell et al., 2014). Collectively they form a major ENE–WSW to NE–SW trending structure which represents one of the inner half-graben/horst structures of the IMFB, known as the Lossiemouth Sub-basin and Central ridge, respectively (Figure 2c; e.g., Andrews et al., 1990). This fault zone can be traced on seismic profiles to within ca. 2.5 km of the southern coastline. Based on the interpretation of seismic reflection profiles, the LFZ has been described as an extensional, southeast-dipping fault with clear Jurassic growth packages developed in its hangingwall (e.g., Figure 2c; e.g., Roberts et al., 1990). The structure, which is steeper in its upper part and dipping more shallowly downwards, has been interpreted by some authors as a reactivated Caledonian thrust (e.g., Barr, 1985).

E–W faults observed onshore between Burghead and Lossiemouth (Figure 2a) represent subsidiary strands of the main offshore trace of the LFZ (Figure 2b; e.g., Al-Hinai et al., 2008; Farrell et al., 2014). This area has been a classic location for studying how fault-related deformation affects the anisotropy of permeability and compartmentalisation of highly porous sandstone as an analogue to similar reservoir rocks in subsurface settings (e.g., Al-Hinai et al., 2008; Edwards et al., 1993; Farrell et al., 2014).

3 | DATASET AND METHODS

3.1 | Onshore analysis

The field data described in this study focus on the brittle deformation associated with the LFZ recorded in the Permo–Triassic rocks cropping out along the southern coast of IMFB between Burghead and Lossiemouth (Figure 2a). Grid references used refer to the British National Grid. Detailed field observations and measurements of bedding, faults and fractures were taken using both a compass-clinometer and the FieldMove™ digital mapping application on an Apple iPad™ (6th Generation). The sense of fault movement was determined based on offset of stratigraphic markers and/or kinematic indicators such as slickenlines, lineations or grooves. To reduce the uncertainty of digital measurements, these were frequently cross-checked using the compass-clinometer.

Fault-slip data were collected and used to perform a palaeostress inversion. This analysis assumes that fault-slip occurs in the direction of the maximum resolved shear stress (Bott, 1959; Wallace, 1951). Different methods have been developed to invert fault kinematic data and derive palaeostress (e.g., Angelier, 1984, 1990; Michael, 1984; Mostafa, 2005; Spang, 1972). This is achieved by obtaining the orientation of the three principal stresses axes (σ_1 , σ_2 and σ_3 —the maximum, intermediate and minimum principal stresses, respectively) and the stress ratio (R) which is defined as $(\sigma_1 - \sigma_2)/(\sigma_2 - \sigma_3)$, also called the reduced stress tensor. In this study, the fault data were analysed using the Angelier (1990) method implemented in the SG2PS software (Sasvári & Baharev, 2014). This method is a direct inversion that estimates the reduced stress tensor from the fault-slip data and the shear stress magnitudes and orientations (Angelier, 1990). The programme also graphically computes the stress regime based on the stress index (R' ; Delvaux et al., 1997).

Some field data were supplemented by lineament interpretations taken from aerial images. The aerial maps were obtained using EDINA Digimap service, which provides access to high-quality 25 cm vertical ortho-photography available for Great Britain, created and licensed by Getmapping plc. To interpret the visible structural features (fault and fracture), the aerial maps were imported into QGIS where the orientations of the polylines were calculated. The processing and visualisation of the structural measurements (from both field and aerial maps) were carried out using Stereonet 10 (Allmendinger et al., 2012; Cardozo & Allmendinger, 2013). The measurements were graphically represented using both rose diagram plots of azimuth distributions (at 10° sector angles) and equal area stereonet, lower hemisphere projections using poles to planes where appropriate. The contouring was

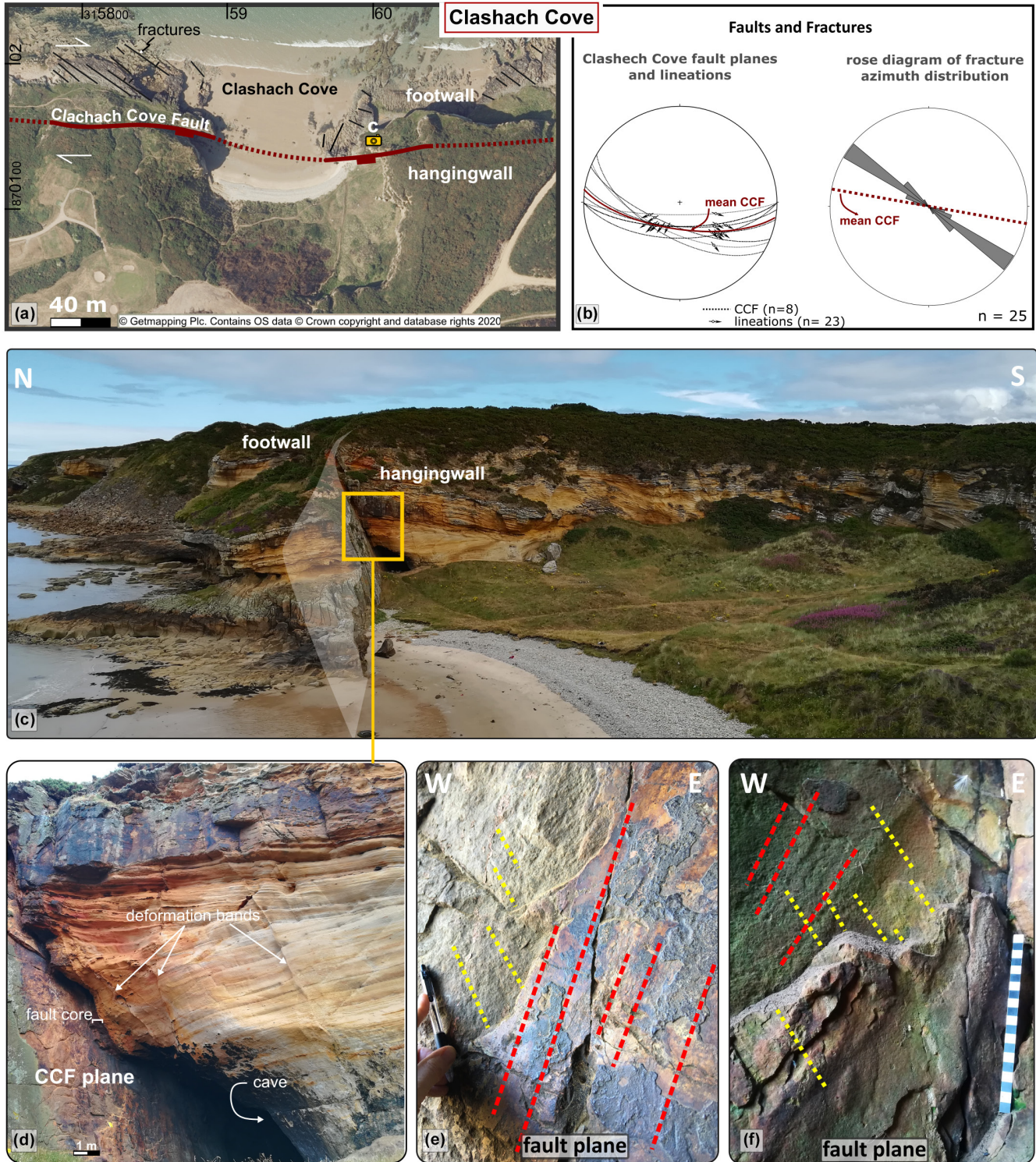


FIGURE 3 Structures observed at Clashach Cove locality (location indicated on [Figure 2a](#)). (a) Aerial map (using EdinaDigimap service © Getmapping Plc) showing the trace of the Clashach Cove Fault (CCF). Fracture traces in fault footwall are shown in black. (b) Stereonets and rose plots of structural data collected in the field. Lower hemisphere, equal area projections. Mean orientation of the CCF is shown. Field photographs showing (c) the CCF cliff exposure on the eastern side of the bay. (d) Close-up of the fault zone looking east. (e–f) Views of CCF plane showing normal oblique-dextral slickenlines (red), polished and iron mineralised nature of fault plane and older, non-mineralised normal oblique-sinistral slickenlines (yellow). In both images, view is towards the fault footwall

done after Kamb (Kamb, 1959) at 2 and 3 sigma standard deviation above a random population.

Oriented fault rock samples were collected from representative outcrop examples during fieldwork for microscopic analysis. Polished thin sections impregnated with blue-stained epoxy were studied and photographed using an optical transmitted and reflected light microscope. These were used to characterise the microstructures and any fault-related mineralisation.

3.2 | Subsurface mapping offshore

The present study used a compilation of 2D regional and 3D time-migrated seismic reflection surveys (Figure 2b). The data are displayed in zero-phase, SEG positive polarity where a downward increase in acoustic impedance corresponds to a positive reflection (red), whereas a decrease corresponds to a negative reflection (blue). The regional 2D seismic lines, acquired in 1997, were provided by Spectrum. Thirty two lines are orientated NW–SE, orthogonal to the main basin-bounding structures of the IMFB (Figure 2b) and have a 2–5 km line spacing. These lines are intersected by eight ENE–WSW-orientated lines with a spacing of 2–14 km. These lines were ideal for regional mapping and for defining the major faults in the basin.

Two 3D time-migrated seismic surveys were also used (Figure 2b). One (*Beatrice 3D*) acquired over the Beatrice Field (e.g., Figure 1b; Linsley et al., 1980) covers an area of 11 × 22 km and has a crossline and inline bin spacing of 12.5 m. The second (*Endeavour 3D*) is located in the central part of the basin, has an area of about 36 × 20 km and a crossline/inline bin spacing of 12.5/25 m, respectively. This high-quality seismic survey allowed a higher-resolution analysis of fault networks and provided insights into the fault kinematics through time. In addition to the seismic reflection data, publicly available (through the National Data Repository) key exploration wells (Figure 2b) were used in this study. Stratigraphic data from boreholes and check-shot/sonic logs allowed determination of the age of the mapped horizons, linking this to the stratigraphic framework for the study area. We also used the velocity data from the wells to construct a velocity model and perform depth conversions where necessary to provide estimates of fault throws and stratigraphic thicknesses. The seismic reflection sections presented here are still shown in TWT, however.

The seismic interpretation was performed using Petrel software. The geometrical interpretation of the seismic horizons has been performed by 2D/3D manual interpretation, and 2D- and 3D-guided autotracking. Three key

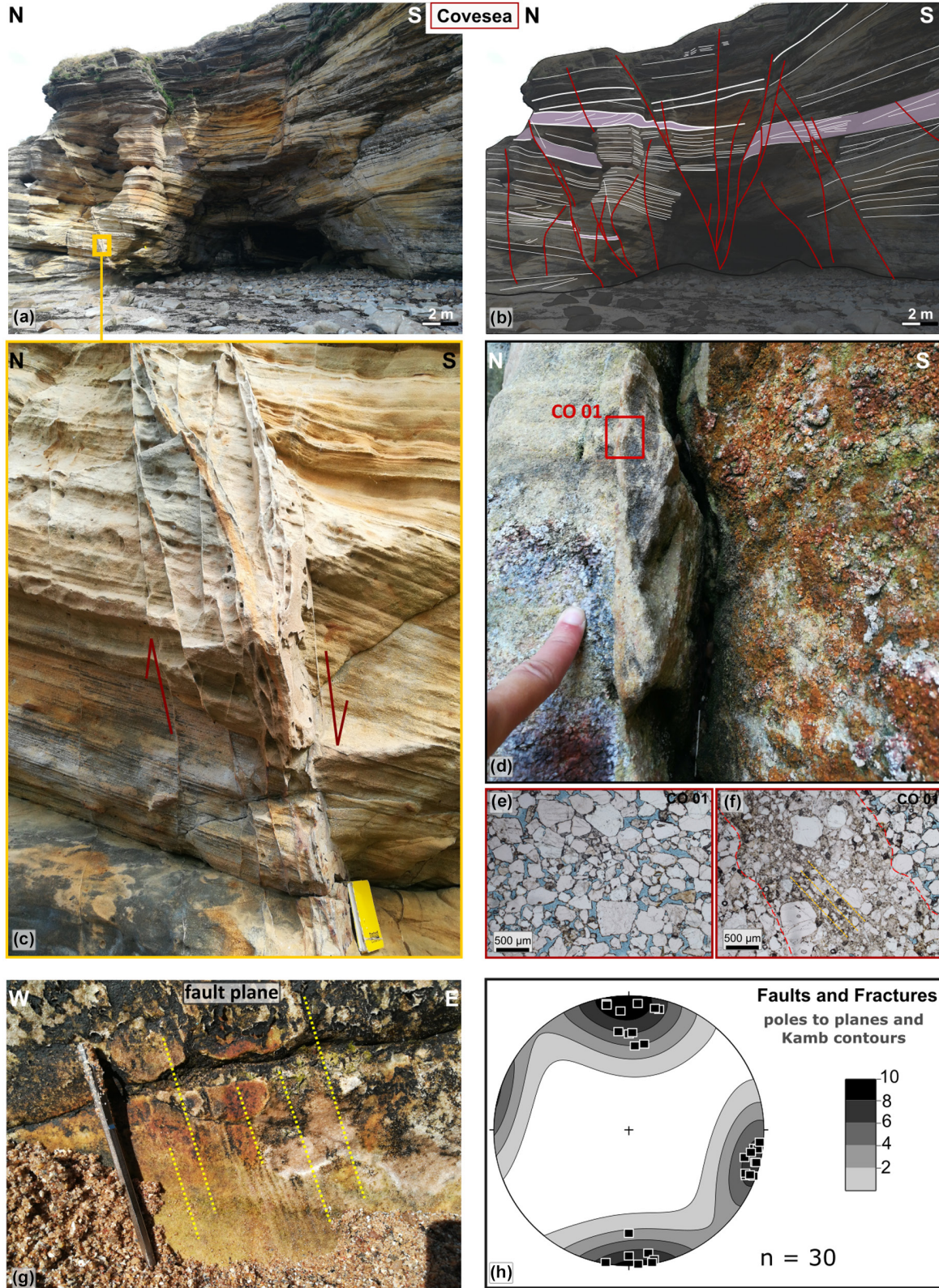
horizons have been selected to illustrate the basin fill architecture and structural history, and to link this to the onshore interpretation. These are as follow: the Variscan unconformity (labelled Variscan UNC on figures), the Stotfield Chert and the NBCE (Figure 2c; see also Figure S2c). We used the interval velocity (v) information from the wells and dominant frequency (f) of the seismic data to approximate the vertical resolution of the mapped horizons ($\lambda/4$, where λ (wavelength) = v/f ; e.g., Brown, 2011). This leads to a limit of separability of ca. 21–23 m for the NBCE, ca. 35 m for the Stotfield Chert and ca. 55–62 for the Variscan UNC.

Two-way time (TWT) structural maps and a TWT thickness map were generated to support structural interpretations. Multiple seismic attribute analyses were carried out on the interpreted surfaces based on the 3D reflection seismic data to assist fault interpretation and enhance small-scale fault detection and visualisation. Seismic attributes have proven to be amongst the most useful geophysical tools to highlight geological features and are routinely used to characterise fault and fracture networks (e.g., Chopra, 2009; Chopra & Marfurt, 2007; Di & Gao, 2017). In this study, we used Variance, Edge Detection and Influential tools. In addition, horizon flattening was performed on key seismic horizons. Variance is possibly the most used attribute in structural interpretation and is highly recommended for the identification of faults and fractures (e.g., Koson et al., 2014; Pigott et al., 2013). This attribute measures the discontinuities in the horizontal continuity of amplitude. Therefore, it converts a volume of continuity (the normal reflections) into a volume of discontinuities in the seismic data, hence highlighting faults or stratigraphic features (e.g., channels; Figure 2.4a; e.g., Brown, 2011; Koson et al., 2014).

Edge detection is a geometrical attribute that can be generated on a map using ‘structural operation’. This will create a property on the data object that highlights sharp edges where subtle changes in the surface topography occur. It can be used either to rapidly highlight a fault network, or to identify potential low throw structures not immediately discernible in the seismic sections (Figure 2.2c; Petrel, 2021).

The influential tools operation generates a property on the map that highlights areas of rapid 3D geometric variation. The points highlighted in this way identify areas within the data set that are prominent influences on the 3D form of the data object (Figure 2.4b; Petrel, 2021).

Horizon flattening is a fast and straightforward tool implemented in Petrel to undo deformation (such as tilting, folding or faulting) and reconstruct geometries to allow better horizon correlation across faults or interpret geometries in the underlying sediment packages.



4 | RESULTS

4.1 | Onshore fieldwork and microscopy

We focus here on four locations at which representative sequences of events and a variety of brittle deformation

styles have been encountered. The localities—Clashach Cove, Covesea, Hopeman East and Branderburgh—all lie along the southern coast of the IMFB, between Burghead and Lossiemouth (Figure 2a). Large areas of Hopeman Sandstone crop out here, together with limited exposures of Stotfield Chert and Upper Devonian (Old Red

FIGURE 4 Structures observed at Covesea locality (location indicated on [Figure 3a](#)). (a) Field photograph and (b) line drawing showing a cross-sectional view looking east at the E–W striking conjugate faults. Some marker beds which could be traced across faults are shown in purple. (c and d) Detailed views of the deformation bands associated with the E–W faults. Location of sample CO 01 shown on (d). (e) Thin section of typical undeformed Hopeman Sandstone impregnated with blue resin to highlight porosity. Rounded to sub-rounded clasts are dominated by quartz and are typical of aeolian sandstones—note haematite rims around clasts. Image in ppl. (f) Thin section through typical deformation band (margins highlighted in red) showing grainsize reduction due to cataclasis and marked reduction in visible porosity due to cementation. The central region shows a weak foliation (highlighted in yellow) due to the onset of pressure solution and possible shearing of grains during faulting. Image in ppl. (g) South-dipping fault plane viewed towards footwall showing normal oblique-sinistral slickenlines indicated by yellow dotted lines. (h) Stereonet of faults and fractures. Lower hemisphere, equal area projection

Sandstone) strata ([Figure 2a](#)). The Hopeman Sandstone displays widespread examples of aeolian cross-bedding (e.g., [Peacock et al., 1968](#); [Maithel et al., 2015](#) and references therein), which are locally modified by both soft-sediment ([Glennie & Hurst, 2007](#)) and later brittle deformation structures. The brittle deformations range in scale from deformation bands with offsets of millimetres to faults with many metres to tens of metres of displacement, which juxtapose different rock formations (e.g., the Burghead Fault; [Figure 2a](#)). The area has been widely used for studying how fault-related deformation affects the anisotropy of permeability and compartmentalisation of highly porous sandstone as an analogue to similar reservoir rocks in subsurface settings (e.g., [Al-Hinai et al., 2008](#); [Edwards et al., 1993](#); [Farrell et al., 2014](#)).

4.1.1 | Clashach Cove [Grid Reference NJ 15978 70131]

The Clashach Cove locality ([Figure 3](#)) is located 2 km east of Hopeman village [NJ 146 694] ([Figure 2a](#)). Hopeman Sandstone is well exposed in both the cliffs and flat-lying rock platforms ([Figure 3a,c](#)). The E–W trending Clashach Cove Fault ([Figure 3a–c](#)) is the best exposed and most accessible seismic-scale fault in the area ([Farrell et al., 2014](#)). It is especially well exposed in the cliffs on the eastern side of the bay ([Figure 3c](#)), displays an E–W trend (270° – 295°) and dips steeply (60° – 80°) towards the south. The fault can also be observed on the western side of the bay (see [Figure S3](#)) and can be traced laterally for over 1 km. However, the best exposure is limited to the sides of the bay, elsewhere is covered by vegetation and difficult to access. The fault throw has been estimated to be no more than 50 m, based on the stratigraphy encountered by a nearby well ([Quinn, 2005](#)).

The fault has a well-developed, 20–50 cm thick, fault core consisting of a heavily iron-stained brown/orange, poorly cemented fault gouge ([Figure 3d](#)). The fault is surrounded by ca. 1-m-wide damage zone dominated by centimetre- to diameter-spaced deformation bands that are individually millimetre-wide, which decrease in density

away from the fault core (see [Farrell et al., 2014](#) for further details).

The footwall fault plane, which is exposed over a lateral extent of 50 m on the east side of the bay, of which 20 m are inside a cave, preserves several polished iron oxide-stained fault-slip surfaces that display a dominant set of slickenlines suggesting normal- (slightly) dextral oblique-slip movements (pitching between 70° and 80° W, [Figure 3e](#); see also [Farrell et al., 2014](#)). A previously undocumented (to our knowledge) set of lineations are also preserved on older, less polished fault planes that consistently display normal-sinistral oblique-slip kinematics (pitching between 50° and 60° E; [Figure 3e,f](#) in yellow). Careful observations using a hand lens show that these are locally overprinted by the dextral normal slickenlines. This observation suggests that the Clashach Cove Fault had more than one episode of movement ([Figure 3e,f](#) in red; see also [Figure S3e,f](#)).

Immediately north of the Clashach Cove Fault, in the flat-lying platform, multiple steeply-dipping (70° – 90°) iron oxide-stained tensile fractures are seen mostly trending WNW–WSE ([Figure 3a](#) black lines). These tensile fractures which strike at ca. 30° – 40° to the Clashach Cove Fault appear to be consistent with the later minor dextral component of shear and associated iron oxide mineralisation along the master fault.

4.1.2 | Covesea [Grid Reference NJ 17841 70835]

This study site ([Figure 4](#)) of about 1 km in length is located 500 m north of Covesea village [NJ 186 704] ([Figure 2a](#)). The Hopeman Sandstone exposed here crops out predominantly in coastal cliffs (ca. 15–20 m high), which locally erode to form systems of caves and natural arches (e.g., [Figure 4a](#)). The sandstones that preserve aeolian cross-bedding have been dissected by numerous faults, deformation bands, fractures and fracture corridors ([Figure 4a–d](#)). The structures here have two main trends ([Figure 4h](#)). The most prominent fault set (e.g., [Figure 4a,b](#)) forms as apparently conjugate faults striking E–W and dipping

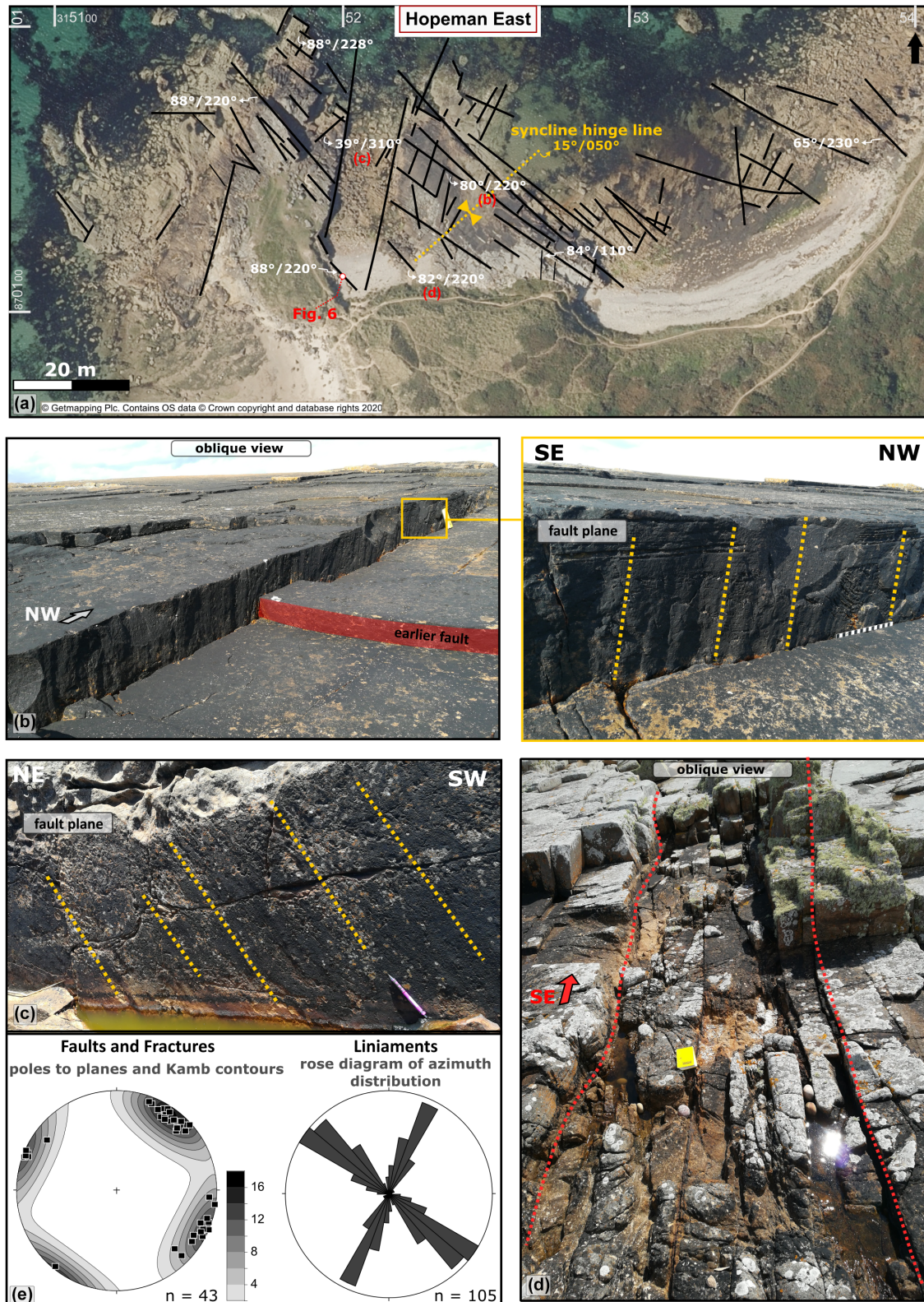


FIGURE 5 Structures observed at Hopeman East locality (location indicated on Figure 3a). (a) Aerial map (using EdinaDigimap service © Getmapping Plc) showing interpreted structural lineaments with representative faults shown as dip and azimuth. Locations of b-d and Figure 6 also indicated. Field photographs showing (b and inset) Oblique view of an NW-SE trending fault showing dip-slip slickenlines. (c) NW-dipping fault plane showing normal oblique-sinistral slickenlines indicated by yellow dotted lines. (d) Oblique view of an NW-SE trending fracture corridor, margins indicated by red dotted lines. (e) Left—stereonet of faults and fractures. Lower hemisphere, equal area projection. Right—rose diagram showing liniaments interpreted from the aerial map

60°–80° to the north and south (Figure 4h). These faults are associated with damage zones in which well-cemented deformation bands develop (Figure 4c,d). The deformation bands are individually 1–10 mm wide and commonly form clusters of up to 30 cm thick (Figure 4c). They are widely associated with slip surfaces accommodating small normal throws ranging from a few millimetres to 20 cm. Exposed S-dipping-slip surfaces locally preserve steeply E-pitching slickenline lineations indicating a sinistral-normal oblique-slip shear senses (pitch 65 E in Figure 4g).

Thin sections show that the undeformed host sandstone is mainly formed by rounded to sub-angular quartz grains with subordinate (<10%) feldspar and metamorphic clasts (mostly mylonitic quartzites; Figure 4e). All clastic grains are coated with thin films of iron oxide (Figure 4e,f; see also Figure S4e,f). Some quartz cementation and overgrowths are present, leading to a porosity reduction (Figure 4e). The effects of cataclasis related to E-W deformation band development are widespread, leading to significant and variable degrees of grain size reduction, compaction and cementation that is typical of such features (e.g., see Fossen et al., 2007; Underhill & Woodcock, 1987). These processes lead to large decreases in porosity (Figure 4f). Some more deformed regions of cataclasis have additionally developed an incipient foliation due to the weak development of solution seams and possible alignment of grains due to shearing (Figure 4f).

The other set of structures is represented by fractures and m-wide fracture corridors striking N–S. These N–S trending fractures, which often form fracture corridors are vertical to steeply dipping (>80°) opening mode tensile fractures which are not associated with deformation bands and show no clear offsets of bedding. Also, these faults are not associated with iron oxide mineralisation.

4.1.3 | Hopeman East [Grid Reference NJ 15176 70163]

This location lies 500 m east of Hopeman village harbour (Figure 2a). The Hopeman Sandstone crops out in a flat-lying wave-cut platform that covers an area of about 250 m by 60 m (Figure 5a). The strata dip sub-horizontally to 15° and appear to be gently folded into an open, gently NE-plunging syncline (15°/050; Figure 5a). It is unclear if this folded geometry is due to tectonic deformation or reflects the presence of large-scale dune cross bedding in the area.

The dominant structures observed both on aerial photographs (Figure 5a; see also Figure S5a) and in outcrops are NNE–SSW and NW–SE trending (Figure 5e). The NNE–SSE trending set (mean vector trending 025°) is represented mainly by steeply dipping to sub-vertical (70°–90°) tensile joints. The NW–SE trending fracture set

(mean vector trending 125°) are formed by steeply dipping (73°–88°) single fractures or fracture corridors of about 1 m wide formed by clusters of closely spaced fractures (Figure 5d) as well as small-scale normal faults (Figure 5b and inset). The fault surfaces display down-dip slickenlines and grooves indicating dip-slip motion. The faults have decimeter-scale offsets and are locally associated with the development of narrow (millimetre wide) deformation bands. NW–SE trending faults appear to locally cross-cut and offset the NNE–SSW structures (Figure 5b) and could be younger. Rare examples of NE–SW trending faults are also present with moderate NW dips (40°) and oblique slickenlines indicating normal-sinistral oblique-slip kinematics (pitch 70°SW; Figure 5c).

The NW–SE trending faults/fractures are distinctively associated with iron oxide mineralisation that is widely observed throughout the Hopeman Sandstone in the coastal sections as both diffuse patches and locally as veins up to 5 mm thick (e.g., Figure 6a,b). Thin sections show that the predominant iron mineral is haematite which locally almost completely occludes the pore space in otherwise high porosity sandstones (Figure 6c). Zoned haematite veining and pore-hosted mineralisation are clearly contiguous and contemporaneous, with mineralising fluids locally extending out into surrounding wall rock pores (Figure 6d). Iron oxide mineralisation post-dates local quartz overgrowths (Figure 6e) and has no associated grain-scale deformation.

4.1.4 | Branderburgh [Grid Reference NJ 23021 71278]

This coastal exposure of about 200 m north of Branderburgh village (Figure 2a) exposes the eastern end of the Burghead Fault. Regionally, the 11-km-long fault strikes E–W and dips moderately to steeply to the south, extending from Burghead to Lossiemouth (BGS, 1969; Edwards et al., 1993). It displays a maximum south-side-down displacement of 275 m (Quinn, 2005), being one of the largest onshore regional faults in the area. The fault juxtaposes Upper Devonian Old Red Sandstone to the north against Upper Triassic Stotfield Chert to the south (Figures 2a and 7a).

The E–W trending (080°) fault is exposed in the tidal zone dipping 55° S and is best viewed at low tide where it can be traced for about 500 m along strike (Figure 7a). Kinematic indicators are not preserved due to weathering of the locally exposed fault plane. The Devonian strata in the footwall are shallowly dipping (20°–35°) to the ESE (Figure 7a) and are represented by well cemented, medium to coarse-grained, red coloured sandstone with sparse deformation bands (Figure 7b). The

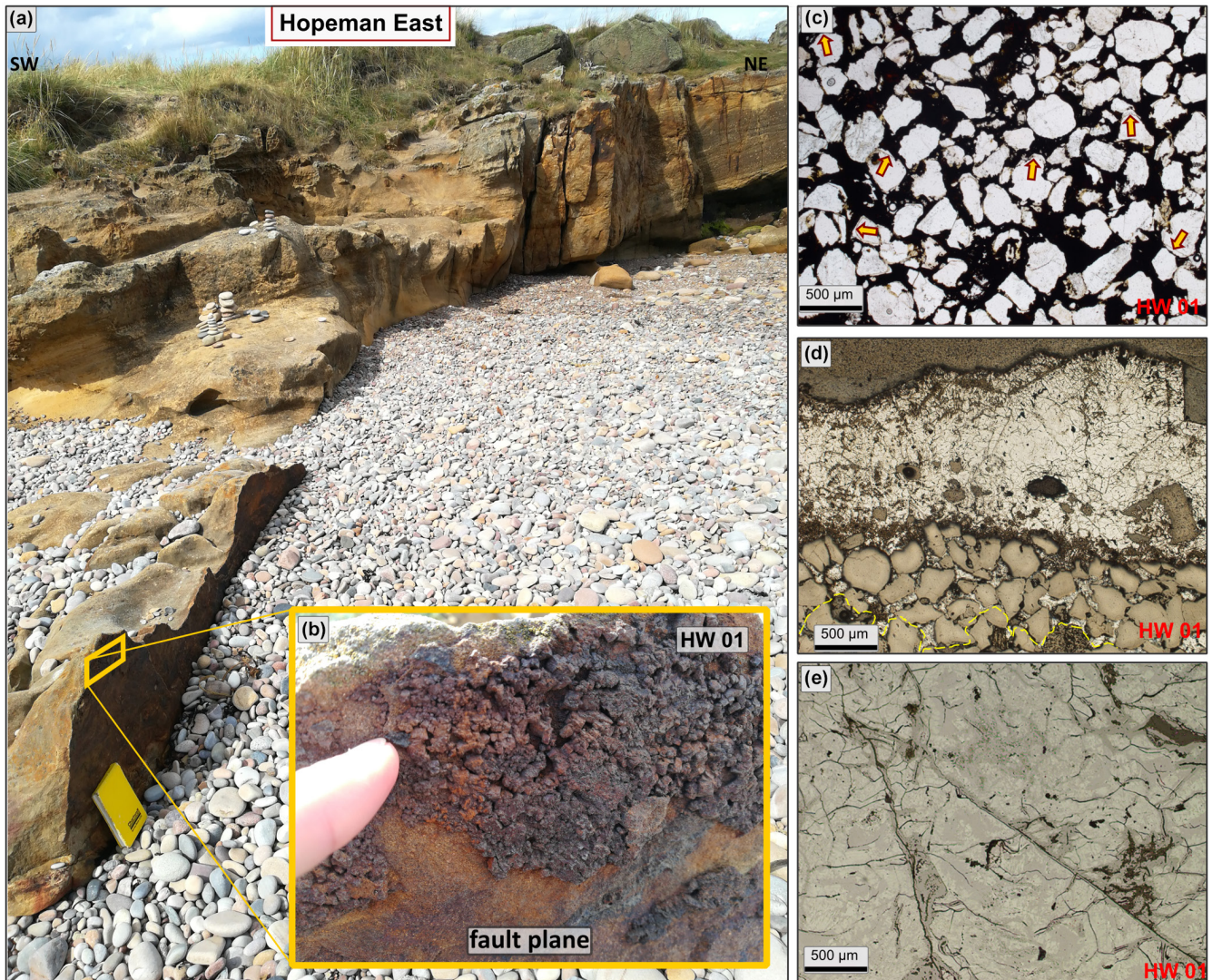


FIGURE 6 Structures observed at Hopeman East locality (location indicated on [Figure 5a](#)). (a and b) Field photographs showing an NW-SE trending iron mineralised fault plane with location of sample HW 01 indicated on (b). (c) Thin section of hematite-stained undeformed Hopeman Sandstone showing how mineralisation has occluded porosity (compare with [Figure 4e](#)). Iron mineral fills post-date quartz overgrowths on clastic grains (examples highlighted by yellow arrows). Image in ppl. (d) Thin section of zoned hematite vein (shown in (b)) in reflected light with mineralisation (bright grey) extending into the pore spaces of the wall rock sandstone, with approximate limit shown by yellow dashed line. (e) High magnification thin section view of mineral vein in reflected light showing hematite (brightest grey) altered to limonite (darker greys) along fracture networks

poorly exposed Upper Triassic strata (Stotfield Chert) in the hangingwall is shallowly dipping (17°) to the east. It has been highly fractured ([Figure 7c](#)). A small cliff exposure located about 100 m south from the contact shows that the formation is cross-cut by E-W trending faults dipping 65° to 75° to both the north and south. Lineations preserved on exposed fault panels here indicate oblique-slip senses of fault movement (pitch 40° W, [Figure 8d](#)). Although the movement direction of this fault cannot be interpreted with confidence, all the faults with this trend seen elsewhere onshore have a component of normal slip. Based on this observation, we infer normal oblique-dextral kinematics.

4.1.5 | Summary of onshore observations

E-W to NE-SW, NW-SE and NNE-SSW trending faults and tensile fracture (joint) sets dominate the onshore exposures of mainly Hopeman Sandstone. The E-W to NE-SW trending faults occur from regional scales (e.g., Clashach Cove Fault; [Figure 3](#)) to minor faults (e.g., [Figure 4](#)). They preserve evidence for early normal-sinistral oblique kinematics (e.g., [Figures 3f](#) and [4g](#)). Minor E-W trending faults developed in the hanging wall of the regional Burghead Fault show normal-dextral oblique kinematics ([Figure 7d](#)), whilst the regional-scale E-W Clashach Cove Fault preserves widespread evidence for a later phase of

normal-dextral oblique kinematics (Figure 3e,f) in addition to an earlier normal-sinistral oblique-slip movement (Figure 3e,f). NW–SE trending fractures and faults show mainly dip-slip normal kinematics (Figure 5b), whilst NNE–SSW opening-mode tensile fractures and fracture corridors are generally not associated with kinematic indicators and are possibly earlier than local NW–SE trending structures based on cross-cutting relationships (Figure 5b).

4.2 | Subsurface offshore interpretation

We focus here both on the high-resolution segment of the LFZ offshore, where the Endeavour 3D seismic volume covers the fault, and regionally in the IMFB to illustrate the structural history and support interpretations made locally in the 3D volume.

Structures associated with the offshore continuation of the LFZ were interpreted using a series of 2D seismic profiles and key seismic horizons maps referring to the three main stratigraphic sequences (Figure 2c). The oldest is the *Permo–Triassic sequence*, bounded by the Variscan unconformity and the Stotfield Chert (Figure 2c-III). This package should preserve evidence of Permian and/or Triassic basin filling and rifting processes (if any). The overlying *Jurassic–Lower Cretaceous sequence* (Figure 2c-II) between the Stotfield Chert and the NBCE should highlight the main periods of syn-rift faulting associated with the main phase development of the IMFB. The uppermost package (Figure 2c-I) is the *post-NBCE sequence* and should highlight post-rift basin filling and any deformation processes associated with (possibly) Cenozoic events.

4.2.1 | Permo–Triassic sequence

The Variscan unconformity is locally characterised by a strong seismic reflector (e.g., Figure 8a; Figure S8a). A few wells have penetrated to the base of the succession (e.g., well 12/29-2, Figure 1c), some of which are located close to the studied seismic profiles, which provides enhanced confidence on the mapping of this seismic horizon.

Regionally, the Stotfield Chert at the top of the Triassic succession forms a strong, laterally continuous seismic marker horizon (e.g., Figure 2c, Figure S2c). Faults observed cross-cutting the Permo–Triassic stratigraphy also displace younger stratigraphy (e.g., Figures 2c, 8a and 9a). Local thickness variations of the Permo–Triassic succession, seen in both the wells and on seismic profiles, have led some authors to suggest that this is due to growth faulting during a Permo–Triassic phase of rifting in the IMFB (e.g., Frostick et al., 1988; Roberts et al., 1989). It is

undoubtedly true that thickness variations in the Permo–Triassic fill are seen in many seismic sections (e.g., Figures 8 and 9). However, the regional Permo–Triassic isochron map (Figure 8c) shows a gradual eastward increase in overall thickness across the study area, but unambiguously fault-controlled thickness variations are not observed at a regional scale (Figure 8c). The Variscan unconformity commonly displays a series of palaeotopographic highs and lows that are infilled by the overlying Permo–Triassic sequence (e.g., Figure 9a,b), which therefore shows large thickness variations (between 200 and 500 ms/ca. 200 and 600 m). Apart from a gentle folding and the presence of small throw (ca. 65 ms/ca. 90 m) faults that cut the stratigraphy up to the surface, the sequence appears largely undeformed (Figure 8a,b). Horizon flattening was performed at the Stotfield Chert level (Figure 8b) to better identify any evidence of Permo–Triassic deformation. This horizon was selected as it is interpreted as a regional palaeosol layer, associated with an overall period of tectonic quiescence (Naylor et al., 1989); hence any Permo–Triassic deformation should have ceased by that time. The resulting basin fill geometry shown in Figure 8b shows that the intra-Permo–Triassic reflectors are consistently sub-parallel and are clearly onlapping the palaeotopographic highs displayed by the basal Variscan unconformity.

Other seismic reflection sections show Permo–Triassic packages apparently ‘wedging’ towards the SE (e.g., Figures 8d,f and 9a,c; see also Figures S8d and Figures S9). After horizon flattening at the Stotfield Chert horizon (Figures 8e,g and 9b,d), however, it is clear that the intra-Permo–Triassic seismic reflectors are sub-parallel and onlap onto the Variscan unconformity. We were unable to find any fault plane reflections or cut-offs which could prove the existence of a fault showing demonstrable Permo–Triassic fault growth geometries. Thus we suggest that in these cases, the apparent wedging geometry occurs due to onlapping of the palaeotopography at the base of the sequence and that in poor seismic data such features could easily be misinterpreted as growth strata.

4.2.2 | Jurassic–Lower Cretaceous sequence

The regional time structure contour map of the Stotfield Chert (Figure 10a), which is overlain by the Jurassic sequence, is dissected by several major ENE–WSW to NE–SW trending faults (tens of kilometres length). These faults form a series of well-defined horsts and grabens, and define the main structural framework of the IMFB. The SSE-dipping LFZ, located in the southern part of the basin (Figure 1b), has a length of about 68 km and can be mapped to within ca. 2.5 km of the coast (Figure 10a). It has a cumulative maximum throw of about 1100 ms

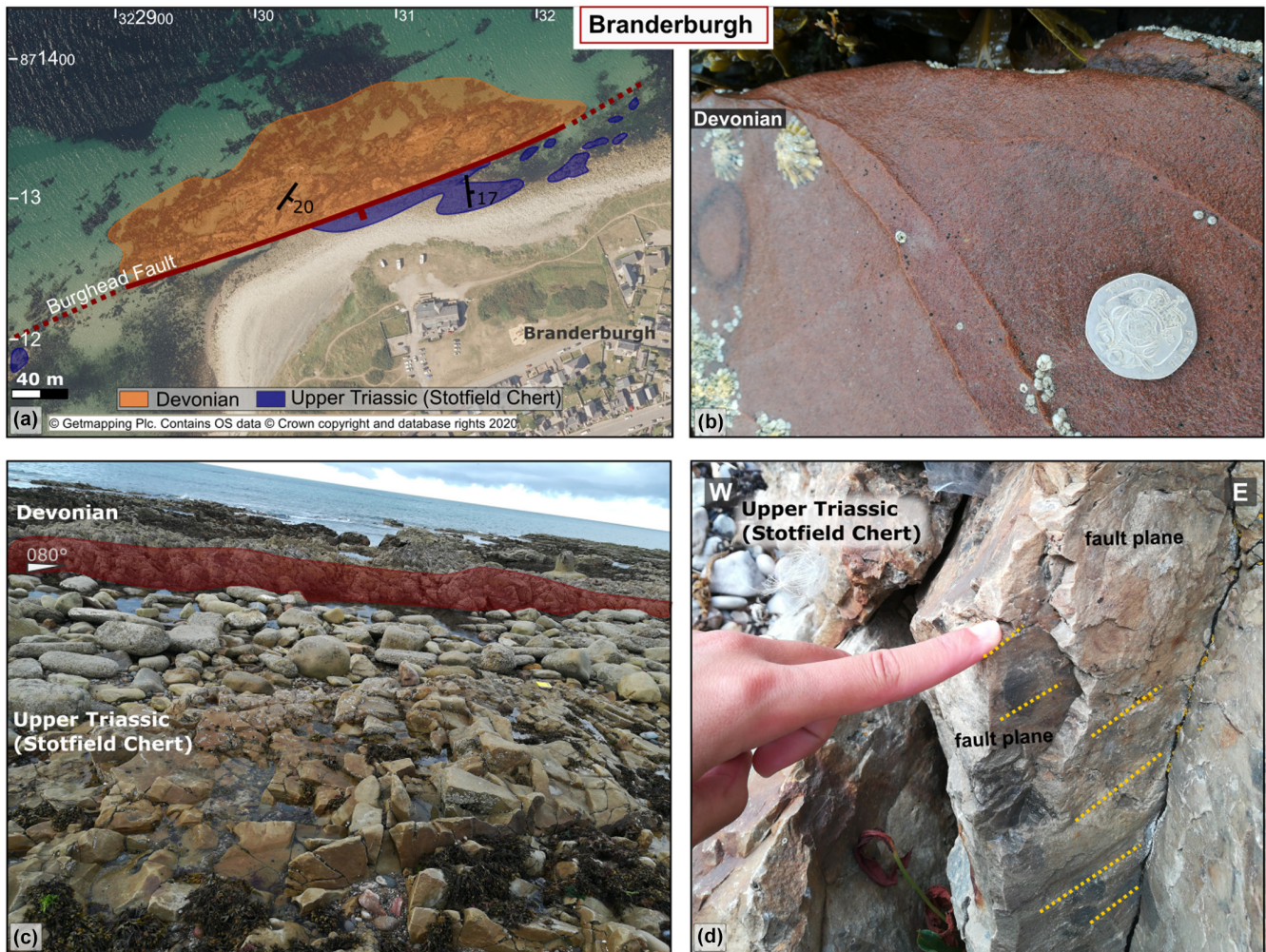


FIGURE 7 Structures observed at Branderburgh locality (location indicated on [Figure 2a](#)). (a) Aerial map (using EdinaDigimap service © Getmapping Plc) showing Burghead Fault and main geological features observed in field. Field photographs showing (b) Devonian sandstone in the footwall of the Burghead Fault. (c) Plan view of Burghead Fault represented as red plane. (d) Cross-section view of faulted Stotfield Chert in the hangingwall of the Burghead Fault. Exposed fault planes show oblique slickenlines indicated by yellow dotted lines

(TWT; ca. 1800 m) recorded at the Stotfield Chert level ([Figure 10b,d](#)). The fault is last intercepted close to the coastline by the IMF97 203 line to the ENE ([Figure 2b](#)), where the fault still has about 223 ms (TWT, ca. 220 m) throw.

The 3D Endeavour seismic survey covers some 28 km length of the LFZ and provides a detailed insight into the fault zone architecture ([Figure 11a](#); see also [Figure S11a](#)). The structure mapped in 3D (at 200 m interval) steeply dips to the SSE ([Figure 11c,d](#)), apparently shallowing at depth ([Figures 10d](#) and [11c](#)). On the high-resolution structural map of the Stotfield Chert horizon ([Figure 11a](#)), it appears that the LFZ consists of two fault segments that link through a breached relay ramp to form a continuous fault array. Minor faults (about 1–5 km in length) trending parallel to the main structure are imaged in both its hangingwall and footwall ([Figure 13a](#)).

Seismic sections oriented approximately perpendicular to the LFZ (e.g., [Figure 10d](#)) show that the Lower and Middle Jurassic strata overlying the Stotfield Chert are characterised by rather parallel reflectors, suggesting an absence of active growth faulting at this time. The overlying Upper Jurassic to Lower Cretaceous succession has a half-graben geometry with a maximum thickness of 750 ms (ca. 1200 m) adjacent to the fault plane ([Figure 10b,d](#)). This shows very clear evidence of syn-tectonic growth faulting in the LFZ hangingwall over this stratigraphic interval.

4.2.3 | Post-NBCE sequence

The Late Jurassic–Early Cretaceous syn-rift sequences are capped by the NBCE, which forms a prominent seismic

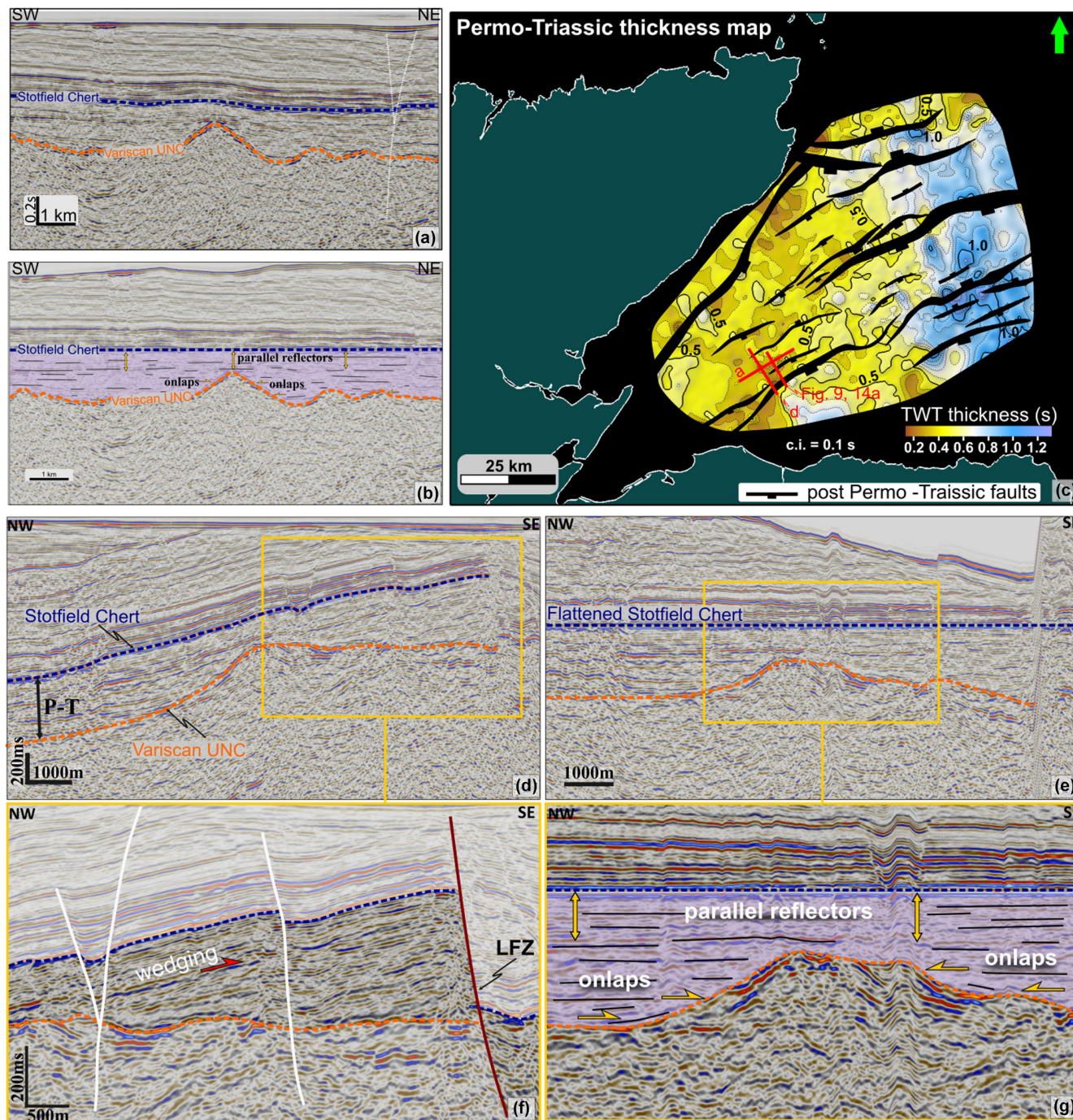


FIGURE 8 (a) SW-NE trending seismic profile showing Stotfield Chert and Variscan UNC horizon. Note the palaeotopographic highs and lows of the Variscan UNC. (b) structural flattened profile at Stotfield Chert horizon showing the Permo-Triassic sequence onlapping the Variscan palaeotopography. Location of (a) is indicated on (c). (c) Regional isochron map between Variscan Unconformity (UNC) and Stotfield Chert showing an increase of Permo-Triassic sequence towards east. Locations of (a), (d) and **Figures 9** and **14** also indicated on the map. (d) NW-SE trending seismic profile with interpretation of Variscan Unconformity (UNC) and Stotfield Chert horizon shown. (e) Structural flattened profile at Stotfield Chert horizon. (f) Enlarged detail of apparent wedging in Permo-Triassic sequence towards the footwall of the Lossiemouth Fault Zone. (g) Enlarged detail from the flattened seismic profile showing the Permo-Triassic sequence onlapping the Variscan palaeotopography

reflector (e.g., **Figure 10e**) that can be confidently mapped across most of the IMFB. On seismic reflection profiles (e.g., **Figure 10d,f**), the LFZ clearly cuts most, if not all, of the stratigraphy up to close to the seabed. The throw

of the NBCE, of about 300 ms (ca. 350 m), is minor compared with the displacement of the Stotfield Chert horizon. Importantly, no thickness variation is observed in the hangingwall of the LFZ to suggest syn-kinematic growth

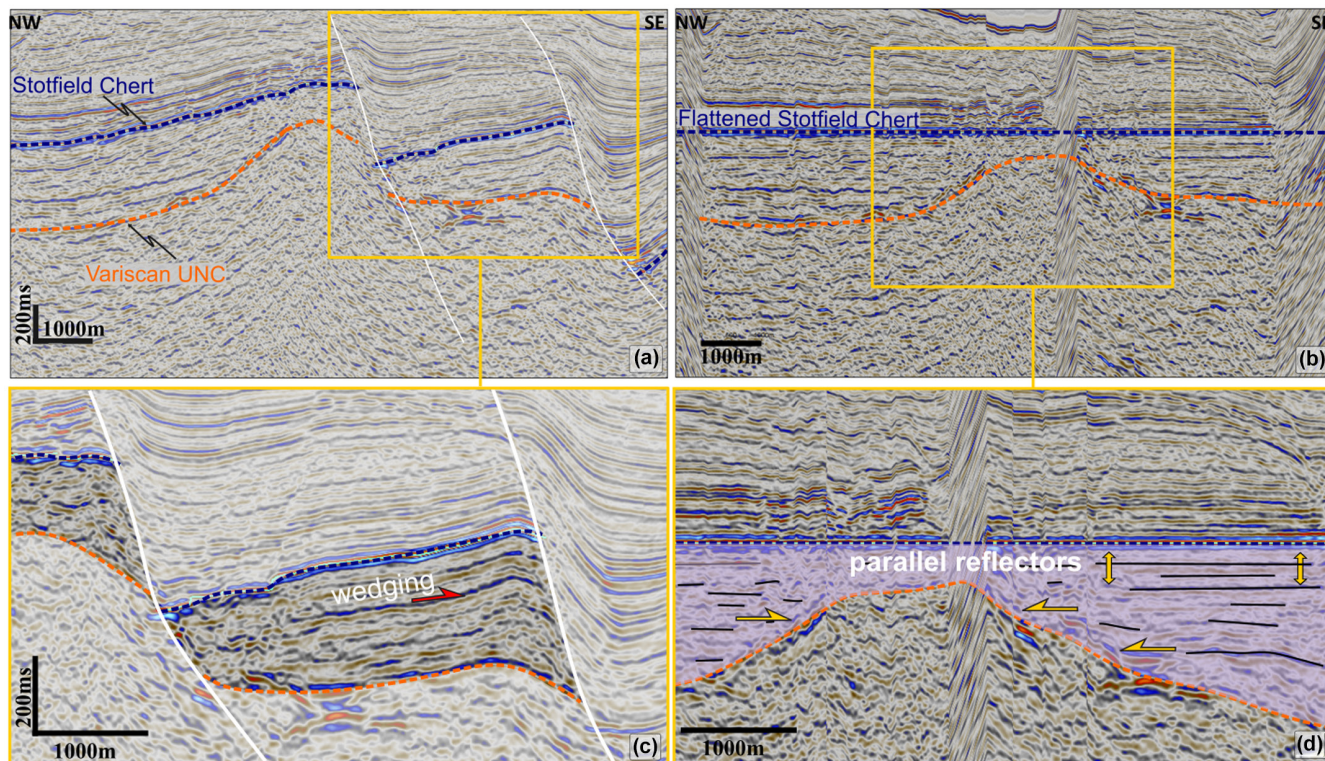


FIGURE 9 (a) NW–SE trending seismic profile (location shown on Figure 8c) with interpretation of Variscan Unconformity (UNC) and Stotfield Chert horizon shown. (b) Structural flattened profile at Stotfield Chert horizon. (c) Enlarged detail of apparent wedging Permo–Triassic sequence towards the footwall of the Lossiemouth Fault. (d) Enlarged detail from the flattened seismic profile showing the Permo–Triassic sequence onlapping the Variscan palaeotopography

(e.g., Figure 10f). Thus, whilst the LFZ cuts through this horizon, the fault was not active during (the preserved) Cretaceous depositional period and was only later reactivated after the deposition of this sequence. More generally within the adjacent Lossiemouth Sub-basin/Central Ridge area (and regionally in the IMFB; Figure 2c), the overlying Cretaceous succession clearly onlaps onto the NBCE horizon, which therefore caps the underlying syn-rift succession (e.g., Figure 10e,f). This suggests that all the faults cutting this horizon post-date the (preserved) Cretaceous sequence.

The regional structural map based on the 2D seismic reflection profiles (Figure 10a) shows that in addition to the LFZ, many other major faults that were active as growth structures during the Jurassic–Early Cretaceous were also reactivated and displace the NBCE horizon. On this regional map, the LFZ appears to be a through-going structure with a mapped strike length of about 40 km (Figure 10a). In the area covered by the Endeavour 3D seismic reflection data, however, the map-view expression of the LFZ becomes much more complex with a series of smaller-scale, en-echelon faults developed, especially towards its northeast termination (Figure 11b; see also Figure S11b).

A well imaged sequence of newly formed, post-NBCE minor faults (lengths <2 km) are seen developed predominantly in the hangingwall of the LFZ (Figures 11b and 12a). We analysed these faults using three seismic structural attributes: ‘Edge detection’ (Figure 12b); ‘Influential data’ (Figure 12c) and ‘Variance’ (Figure 12d), in order to enhance these structures which lie close to the limits of seismic resolution. Three fault populations trending NNW–SSE, NW–SE and WNW–ESE are distinguishable (Figure 12e). These faults include NW–SE trending faults that are mostly associated with the reactivated LFZ and minor newly formed faults in the proximity of the Lossiemouth Fault trending mainly WNW–ESE and NNW–SSE, although other orientations are also present (Figure 12f).

These fault populations are consistent with a dextral strike-slip Riedel system developed during NE–SW extension (Figure 12f). We suggest that the NNW–SSE trending faults (Figure 12e,f, shown in yellow) correspond to antithetic Riedel structures, the NW–SE trending features (Figure 12e,f, shown in blue) to opening mode fractures/normal faults and the WNW–ESE trending faults (Figure 12e,f, shown in dark red) to synthetic Riedel structures. In addition to those main Riedel structures, occasional Y and P shear structures are also observed (Figure 12e).

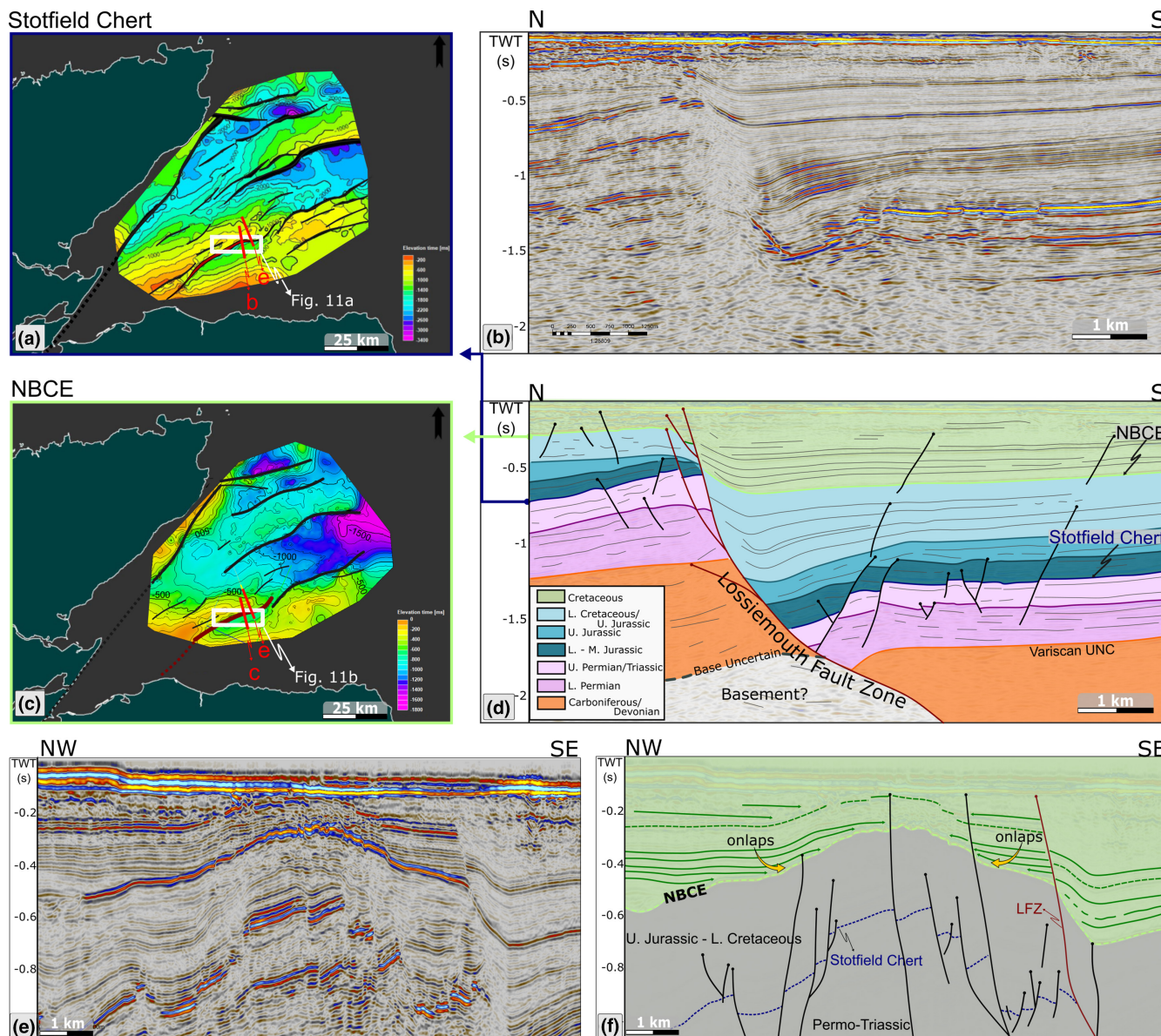


FIGURE 10 Regional TWT structural map of (a) Near Base Cretaceous Event (NBCE) and (b) Stotfield Chert horizon. Lossiemouth Fault Zone is indicated by dark red line. Locations of (c) and (e), as well as Figure 12a, indicated on the map. N-S trending seismic profile through Lossiemouth Fault Zone (c) uninterpreted and (d) interpreted stratigraphy and faults. NW-SE trending seismic profile (e) uninterpreted and (f) interpreted to highlight the onlapping nature of the post-NBCE sequence

5 | DISCUSSION

5.1 | Onshore and offshore development of the LFZ

Based on the offshore interpretation and correlation with the regional events, we suggest that the development of the LFZ had two major episodes. The first episode is related to the main stage of rifting in the IMFB during the Late Jurassic–Early Cretaceous. The second episode is mostly associated with the reactivation of the earlier formed LFZ as well as movements along other regional NE–SW to E–W trending faults in the IMFB (Figure 10c).

The structural relationships associated with the offshore LFZ provide an important insight into how the various fault sets and kinematic patterns may be correlated and separated onshore in terms of their relative age.

5.1.1 | Structures developed during the post-rift reactivation

The offshore data show that the E–W trending LFZ is a composite reactivated structure that is formed by a series of hard and soft-linked subordinate faults especially towards its lateral terminations (e.g., Figures 11b

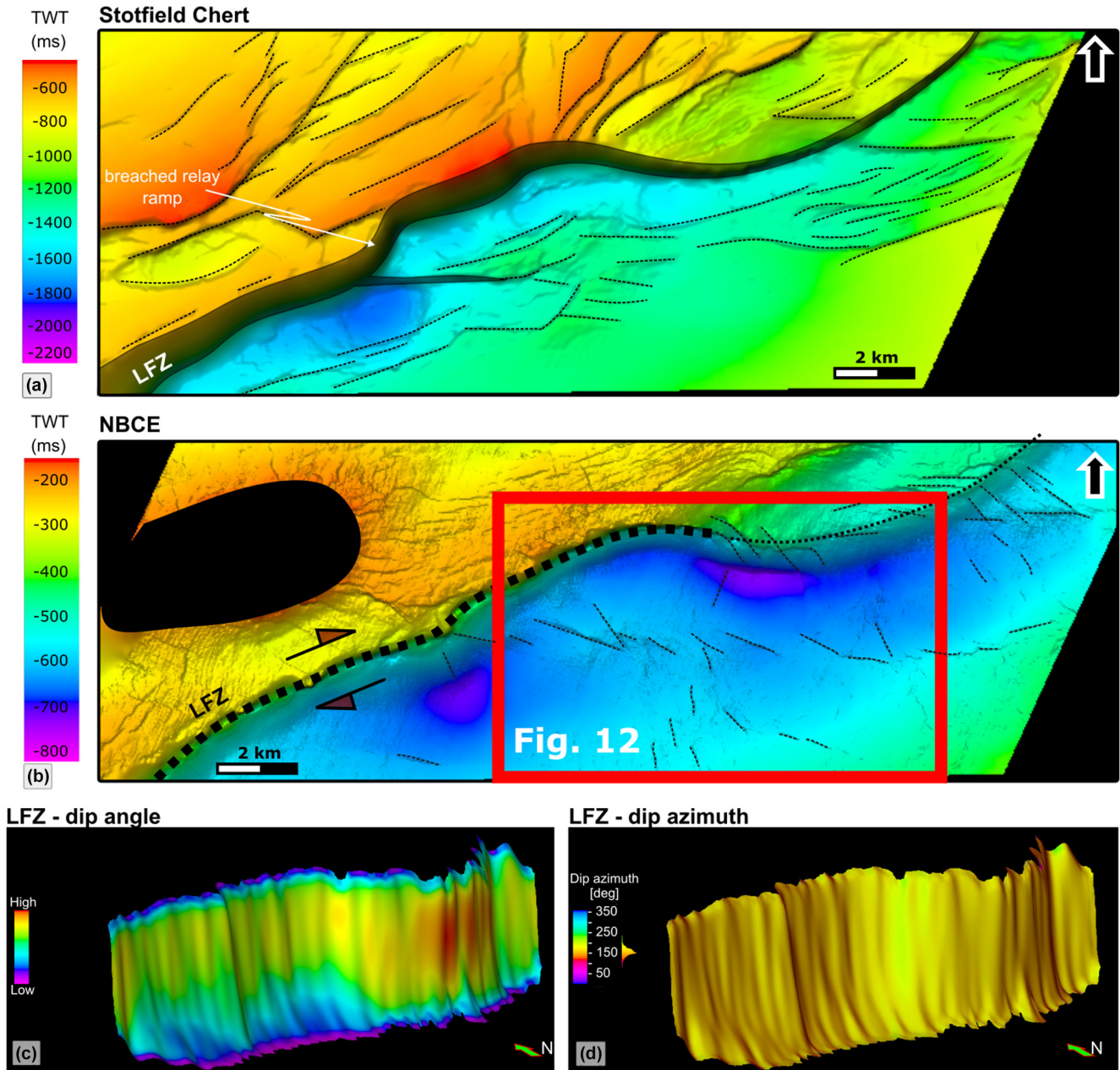


FIGURE 11 Local TWT structural map of: (a) Stotfield Chert horizon; and (b) Near Base Cretaceous Event (NBCE) interpreted based on 3D reflection data along the northeastern end of the LFZ. Dashed black lines represent minor faults on both maps. Lossiemouth Fault surface covered by the 3D data displaying (c) dip angle and (d) dip azimuth attributes

and 12). The interpretation of the well-imaged minor structures, interpreted as Riedel shears, can be used to infer dextral kinematics along the LFZ during NE–SW-directed extension (Figure 12e,f). Based on fault trend and inferred kinematics, we suggest the following correlation with the onshore structures. The E–W to ENE–WSW trending faults (sub-parallel to the Lossiemouth Fault) showing dextral/oblique-dextral kinematics, plausibly represent either dextrally reactivated Late Jurassic–Early Cretaceous rift-related faults or are newly developed synthetic Riedels or Y faults (e.g., like

those in Figure 12e,f, shown in dark red and bright red, respectively) during reactivation. These types could include the later phase of normal-dextral oblique slip seen along the Clashach Cove Fault (Figure 3e). Movements along the Burghead Fault have been previously inferred by Quinn (2005) to be Late Jurassic based mainly on the presence of Lower Jurassic sedimentary rocks in the hangingwall of the fault (Figure 2a). It is possible that this structure did form during the main stage of Late Jurassic–Early Cretaceous rifting. However, the sub-parallel minor faults observed in its hangingwall, which

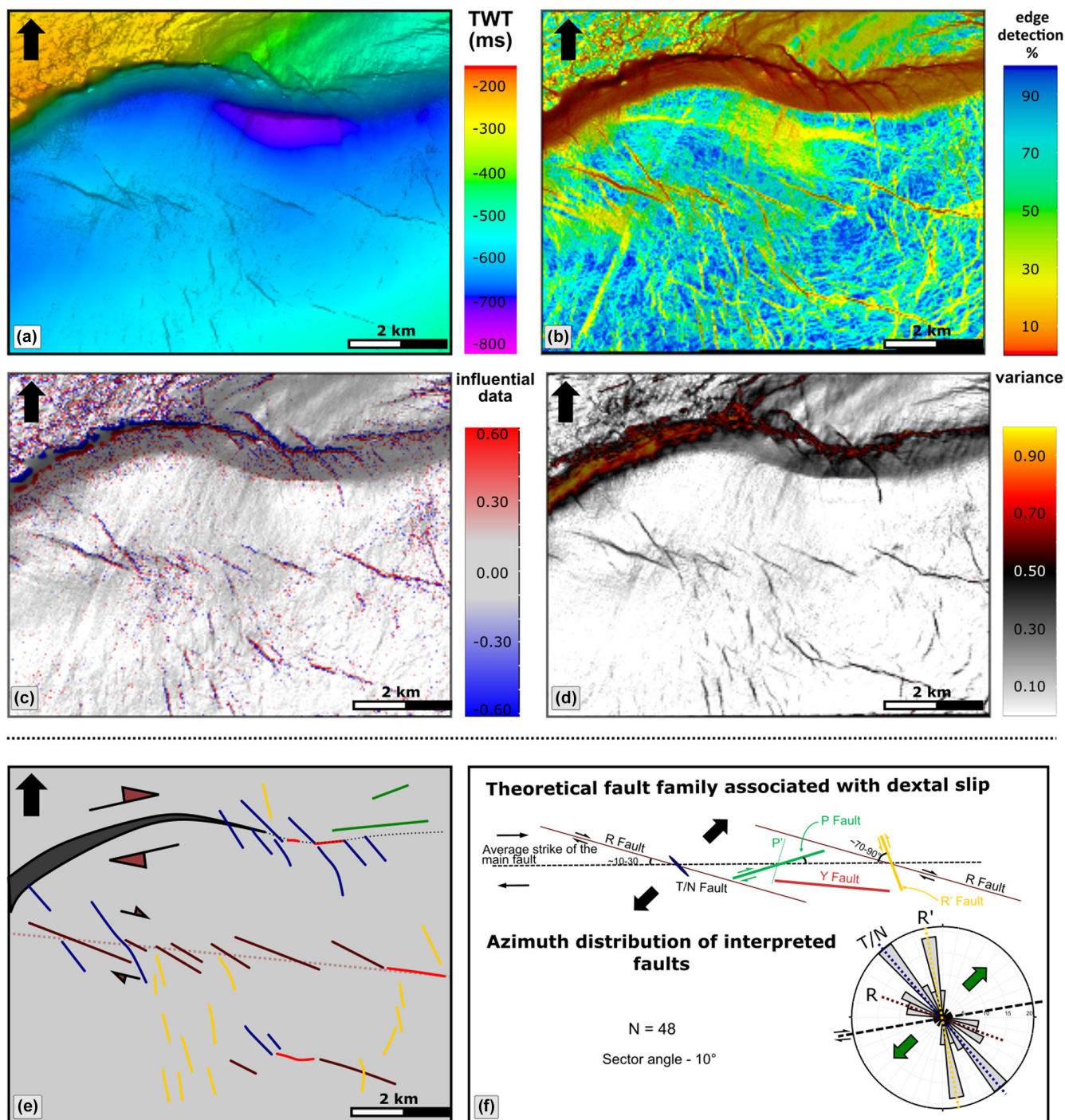


FIGURE 12 (a) Enlarged detail of the Near Base Cretaceous Event (NBCE) TWT map interpreted based on 3D reflection data (see location on Figure 11b). (a–d) Seismic attribute maps enhancing fault/fracture visualisation. (e) Interpreted structures in map view and (f) Rose diagram of azimuth distributions. The fault array geometry suggests a component of dextral movement. Theoretical fault family for dextral strike-slip is shown for comparison in (f), modified after Carne & Little, 2012. Structures are colour coded in both (e) and (f) as follows: grey—main (Lossiemouth) fault; dark red—synthetic Riedels (R); yellow—antithetic Riedels (R'); blue—tensile (T) or normal (N) faults; bright red—Y fractures; green—P fractures

show oblique-dextral kinematics (Figure 7d), could indicate that this fault has also been reactivated or even initiated during this later stage. We further propose that the WNW–ESE- to NW–SE trending structures seen onshore at Clashach Cove (Figure 3a,b) and Hopeman East

(e.g., Figure 5b and inset) represent post-NBCE tensile fractures or dip-slip faults equivalent to those seen offshore (e.g., Figure 12e,f, in blue).

All of these onshore structures are consistently associated with iron oxide mineralisation (e.g., Figures 3e and

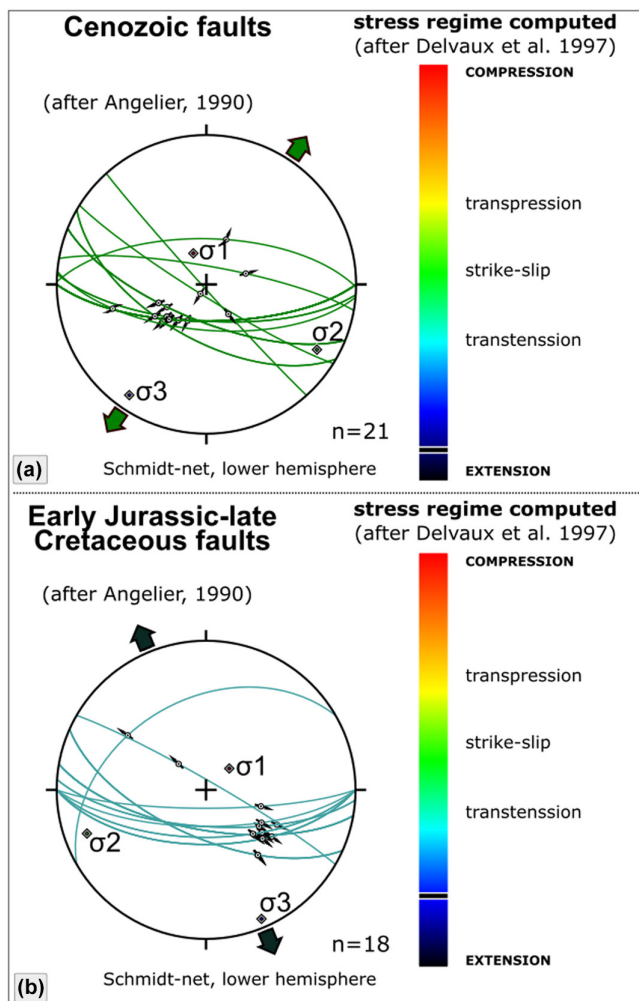


FIGURE 13 Stress inversion plots (after Angelier, 1990) of: (a) oblique-dextral; and (b) oblique-sinistral normal faults from onshore study area—see text for further details

6b). This characteristic and prominent mineralisation event gives confidence that the proposed correlation of structures is robust.

Having grouped these onshore structures and as suggesting that they formed during the post-NBCE stage, we are now able to carry out a stress inversion analysis. This suggests that the faults developed during NNE–SSW extension (Figure 13a) in a regime of near-horizontal extensional stress with a sigma three-axis orientated $09/214^\circ$ and a near-vertical compressive stress with a sigma one-axis orientated $73^\circ/335^\circ$ (Figure 13a). The timing of this faulting and reactivation episode remains uncertain; however, this pattern is consistent with the regional understanding of Cenozoic deformation in the IMFB, which suggest widespread reactivation of intrabasinal structures (e.g., Argent et al., 2002; Farrell et al., 2014; Thomson, 1993; Thomson & Underhill, 1993) due to the dextral reactivation of the Great Glen Fault

(e.g., Le Breton et al., 2013; Thomson & Hillis, 1995; Underhill, 1991).

5.1.2 | Structures developed during the Late Jurassic–Early Cretaceous

The remaining structures seen in the onshore area comprise E–W to ENE–WSW trending faults, sub-parallel with the regional Lossiemouth Fault. These include the earlier phase of normal-sinistral oblique movement seen along the Clashach Cove Fault (Figure 3f), and the normal-sinistral minor faults present at Covesea (Figure 4g) and Hopeman East (Figure 5c). These faults are widely associated with the development of deformation bands (e.g., Figure 4c). Such deformation band arrays are very likely to act as baffles to fluid flow in the subsurface (e.g., Rotevatn et al., 2013, 2016; Shipton et al., 2002).

In the offshore, these fault trends are typical of Late Jurassic–Early Cretaceous syn-rift faults (Figure 11a). Whilst many recent models, based on interpretations of seismic reflection data, tend to suggest that there is little evidence for the development of syn-rift oblique-slip faults in the basin (e.g., Davies et al., 2001; Lăpădat et al., 2016; Long & Imber, 2010), others such as Underhill (1991) suggest that a limited degree of strike-slip movement might be possible along any of the main half-graben bounding faults. Most recently, Tamas et al. (2021) have proposed that limited and hitherto unrecognised transtensional components may be associated with fault reactivation during basin development.

A palaeostress inversion analysis of the slickenline lineations associated with the E–W to ENE–WSW trending structures showing normal-sinistral oblique movements onshore yields an NNW–SSE extension direction (Figure 13b). The faults were developed in a regime of near-horizontal extensional stress with a sigma three-axis orientated $04^\circ/157^\circ$ and near-vertical compressive stress with a sigma one-axis orientated $72^\circ/052^\circ$ (Figure 13b). This extension direction correlates well with the NW–SE extension direction proposed by Davies et al. (2001) based on offshore fault trends during the Oxfordian-early Kimmeridgian period. It is also parallel to the NNW–SSE extension direction seen during later phases of faulting (ca. 131 Ma) in onshore Devonian strata of the Turriff basin located on the southern margin of the IMFB, ca. 70 km east of the study area (see Tamas et al., 2021).

The NNW–SSE to N–S trending faults identified onshore in our study area are also locally visible cutting the top Stotfield Chert map offshore (e.g., Figure 11a). Although we were unable to recognise any kinematic indicators on these structures, Edwards et al. (1993) have described dextral oblique slip on N–S to

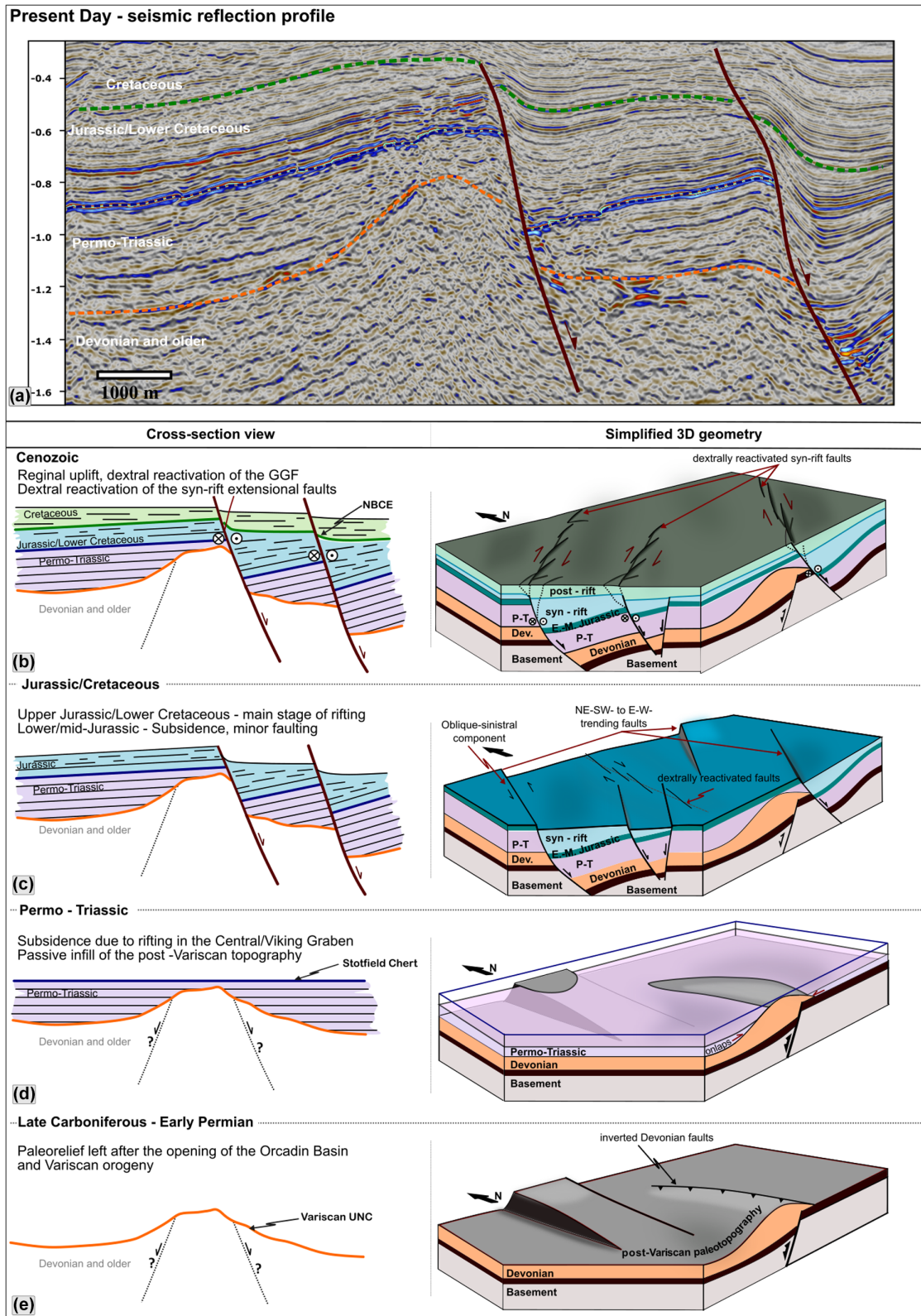


FIGURE 14 Summary of basin development using a representative 2D seismic profile (see location of Figure 8c)

NNE-SSW trending faults in the Cumingstone area, near the western end of Burghead fault (Figure 2a). Such oblique-dextral reactivation along NNE-SSW trending

faults has also been identified in the Devonian strata in the Turriff sub-basin (Tamas et al., 2021). U-Pb calcite dating of syn-kinematic mineralisation associated with

these structures revealed that they likely formed during the Early Cretaceous (130.99 ± 4.6 Ma) under NNW–SSE extension (Tamas et al., 2021). In the Turriff sub-basin, this leads to dextral reactivation of pre-existing N–S to NNE–SSW trending Devonian rift faults and normal-sinistral oblique faulting along E–W to ENE–WSW trending structures.

On the basis of the above observations and correlations, it is suggested that the earlier E–W trending sinistral normal and NNW–SSE to N–S trending, possibly dextral structures are related to the main phase(s) of Late Jurassic to Early Cretaceous rifting during the development of the IMFB. Unfortunately, no syn-tectonic calcite veins which could be dated in order to confirm this suggestion were observed in the area. However, the integrated onshore–offshore approach used here provides an alternative approach that can be used when absolute dating of syn-tectonic mineral fill cannot be undertaken.

5.2 | Structural–stratigraphic relationships associated with the Permo–Triassic

The interpretation of the offshore seismic reflection profiles (Figures 8 and 9) suggests that the Permo–Triassic sequence is largely characterised by onlapping onto a pre-existing post-Variscan palaeotopography and a seismic facies comprising parallel reflectors (e.g., Figure 8b). Apparent wedge-like thickness variations have been shown—after horizon flattening at the Stotfield Chert Formation level and removal of deformation related to younger events—to be artefacts of Late Jurassic–Early Cretaceous and Cenozoic tilting and faulting (e.g., Figure 8e). Coincidentally, wedging is also observed in the footwall of major syn-rift (Late Jurassic–Early Cretaceous) faults (e.g., Figure 9a). This implies that Permo–Triassic faults (presumably) having the same strike directions were not reactivated during Late Jurassic–Early Cretaceous, but were cross-cut by new oppositely dipping faults. Although this is not an impossible scenario in fault development, the lack of seismic evidence of a fault plane (e.g., fault plane reflection) and combined with the results of horizon flattening, which suggest parallel reflectors and onlaps (Figures 8b,g and 9d), we lean towards apparent growth strata. Additionally, Andrews et al. (1990) argue that previously cited Permo–Triassic wedges in the IMFB are, in fact, Devonian and Upper Jurassic sequences.

A passive subsidence and infilling of a pre-existing topography during the Permo–Triassic supports the regional models proposed by Thomson and Underhill (1993) and Andrews et al. (1990). Therefore, we suggest that none of

faults and fractures observed onshore are the product of Permo–Triassic faulting. This is supported by the absence of local variations of the thickness of the Permo–Triassic sequences across the Burghead Fault in onshore outcrops (Quinn, 2005).

6 | CONCLUSIONS

Onshore and offshore studies of the region associated with the LFZ on the southern margin of the IMFB have revealed the presence of NE–SW to E–W, N–S to NNE–SSW and NW–SE striking faults/fractures, creating a complex, composite reactivated structure. An onshore (surface)–offshore (sub-surface) integrated analysis has revealed the following structural history summarised in Figure 14:

1. *Pre-rift*: Interpretations of offshore seismic data and lack of observed changes in sediment thickness across major exposed faults onshore lead us to conclude that the Permo–Triassic basin development was not associated with active faulting, at least in the southern part of the IMFB. The basin at this time was characterised by sag-like regional subsidence and passive infilling of a pre-existing Variscan palaeotopography (Figure 14e,d). Local thickness variations within the Permo–Triassic sequences are related to this infilling process. Later faulting and tilting of these packages can produce wedge-like geometries that may on initial inspection resemble syn-kinematic growth strata, particularly in older, lower resolution 2D seismic sections (e.g., Figures 8f and 9c).
2. *Syn-rift*: Major E–W to NE–SW trending faults develop, including the LFZ (Figure 14c). Offshore, they show a close association with wedge-shaped Upper Jurassic–Lower Cretaceous seismic packages (Figures 10b,d and 14c), confirming their relative timing and syn-rift nature. In the onshore study area, typically normal-sinistral oblique E–W to ENE–WSW trending faults develop under an NNW–SSE extension direction. Such faults include the Clashach Cove Fault (Figure 3f), minor faults at Covesea (Figure 4) and most likely the Burghead Fault (Figure 7a,c). Minor en-echelon, NNE–SSW trending faults also occur (Figure 11a) which could be related to dextral reactivation of deeper Devonian structures as seen onshore in the Turriff basin further to the east (Tamas et al., 2021).
3. *Post-rift*: This likely Cenozoic event is largely associated with the reactivation of the earlier formed major NE–SW to E–W trending fault complexes in the IMFB (Figure 14b). Evidence of fault reactivation is encountered both onshore and offshore. Offshore, the LFZ shows evidence of dextral-normal reactivation, attested

by newly formed minor en-echelon E–W to ENE–WSW, NW–SE, and NNW–SSE to N–S trending faults, interpreted as Riedel structures which fit a dextral reactivation model (Figure 12e,f). Onshore, NNE–SSW-directed extension resulted both in the oblique dextral reactivation of the E–W to ENE–WSW trending faults and the development of other minor dextral E–W to ENE–WSW or dip-slip NW–SE striking faults. All of these movements are associated with widespread iron oxide mineralisation. Major faults such as Clashach Cove Fault have been reactivated during this episode (Figure 3e). This interpretation suggests that the Cenozoic deformation extends to the southern margins of the IMFB and is not simply limited to the north-western shore close to the Helmsdale and Great Glen fault zones (e.g., Le Breton et al., 2013; Underhill & Brodie, 1993).

The present case study demonstrates the prevalence of structural inheritance and fault reactivation during superimposed faulting episodes associated with the geological evolution of the IMFB. It also highlights the value of integrating and correlating onshore surface and offshore subsurface data to better assess the timing and kinematics of basin development. This approach better justifies the application offshore of the strike-slip strain-ellipse model to interpret faulting patterns in plan view since equivalent structures are seen onshore in surface exposures where kinematic evidence for components of dextral and/or sinistral movement is preserved.

More generally, the workflow used here can be adapted to characterise deformation events in other rift or superimposed rift basins. For example, oblique-slip/strike-slip faults may not be well imaged in the subsurface as they require good 3D imaging and commonly refer to distant and remote analogue structures to validate the interpretation. This study shows how a field-calibrated seismic interpretation can aid in recognising fault patterns that can be associated with oblique-slip faults. Complex fault arrays developed due to the oblique reactivation of pre-existing fault are increasingly being documented in the subsurface in other superimposed basins, especially due to the wider availability of 3D seismic datasets; e.g., Gulf of Thailand (Morley, 2016 and references therein); offshore New Zealand (Giba et al., 2012) and NW Shelf of Australia (Deng & McClay, 2021; Deng et al., 2020, 2021).

Finally we have demonstrated that not all apparent wedge geometries identified in seismic data can be reliably correlated with growth strata consistent with syn-kinematic deposition. We hope this study will provide an analogue and inspire seismic interpreters working in other basins to consider both the possibility of apparent growth strata, and the importance of oblique-slip deformation patterns. This will significantly reduce uncertainties in the interpretation of subsurface datasets.

ACKNOWLEDGEMENTS

This research is based on the PhD work of AT undertaken as part of the Natural Environment Research Council (NERC) Centre for Doctoral Training (CDT) in Oil and Gas [grant number NEM00578X/1] and was funded by Durham University and British Geological Survey (BGS) via the British University Funding Initiative (BUFI), whose support is gratefully acknowledged. The seismic interpretation part was undertaken in the Centre for Exploration Geoscience in the Institute of GeoEnergy Engineering (IGE) at Heriot-Watt University (HWU) using Schlumberger's Petrel software released to HWU under academic license. The seismic and well data were obtained from the Oil and Gas Authority's National Data Repository (NDR) and access to Fugro GeoTeam's regional 2D spec survey, both of which are acknowledged. Ian Chaplin and Sophie Edwards are thanked for the thin-section preparation. DMC contributes here by permission of the Executive Director, British Geological Survey, UKRI. Craig Magee, Billy Andrews, and an anonymous reviewer are thanked for their thorough and constructive comments.

PEER REVIEW

The peer review history for this article is available at <https://publons.com/publon/10.1111/bre.12661>.

DATA AVAILABILITY STATEMENT

The data that support the findings of this study are available from Fugro GeoTeam and Oil and Gas Authority. Restrictions apply to the availability of these data, which were used under license for this study. Data are available from the author(s) with the permission of Fugro GeoTeam and Oil and Gas Authority.

ORCID

Alexandra Tamas  <https://orcid.org/0000-0001-8010-1853>

Robert E. Holdsworth  <https://orcid.org/0000-0002-3467-835X>

Dan M. Tamas  <https://orcid.org/0000-0002-6640-8928>

Edward D. Dempsey  <https://orcid.org/0000-0002-8425-2226>

Dave J. McCarthy  <https://orcid.org/0000-0002-0677-773X>

Ken J. W. McCaffrey  <https://orcid.org/0000-0002-9882-1709>

REFERENCES

- Al-Hinai, S., Fisher, Q. J., Al-Busafi, B., Guise, P., & Grattoni, C. A. (2008). Laboratory measurements of the relative permeability of cataclastic fault rocks: An important consideration for production simulation modelling. *Marine and Petroleum Geology*, 25, 473–485.

- Allmendinger, R. W., Cardozo, N., & Fisher, D. (2012). *Structural Geology Algorithms: Vectors and Tensors in Structural Geology*. Cambridge University Press.
- Andrews, I. J., Long, D., Richards, P. C., Thomson, A. R., Brown, S., Chesher, J. A., & McCormac, M. (1990). *The Geology of the Moray Firth*. British Geological Survey.
- Angelier, J. (1984). Tectonic analysis of fault slip data sets. *Journal of Geophysical Research*, 89, 5835–5848.
- Angelier, J. (1990). Inversion of field data in fault tectonics to obtain the regional stress III: A new rapid direct inversion method by analytical means. *Geophysical Journal International*, 103, 363–376.
- Argent, J., Stewart, S. A., Green, P., & Underhill, J. R. (2002). Heterogeneous exhumation in the Inner Moray Firth, UK North Sea: Constraints from new apatite fission track analysis and seismic data. *Journal of the Geological Society*, 159, 715–729.
- Barr, D. (1985). 3-D palinspastic restoration of normal faults in the Inner Moray Firth: Implications for extensional basin development. *Earth and Planetary Science Letters*, 75, 191–203.
- Bell, R. E., Jackson, C.-A.-L., Whipp, P. S., & Clements, B. (2014). Strain migration during multiphase extension: Observations from the northern North Sea. *Tectonics*, 33, 1936–1963. <https://doi.org/10.1002/2014TC003551>
- Benton, M. J., & Walker, A. D. (1985). Palaeoecology, taphonomy, and dating of Permo-Triassic reptiles from Elgin, north-east Scotland. *Palaeontology*, 28, 207–234.
- BGS. (1969). *Geological Map, Elgin Sheet (1:63 360)*. British Geological Survey.
- Bird, T. J., Bell, A., Gibbs, A. D., & Nicholson, J. (1987). Aspects of strike-slip tectonics in the Inner Moray Firth Basin, offshore Scotland. *Norsk Geologisk Tidsskrift*, 67, 353–369.
- Bosworth, W., & Tari, G. (2021). Hydrocarbon accumulation in basins with multiple phases of extension and inversion: Examples from the Western Desert (Egypt) and the western Black Sea. *Solid Earth*, 12, 59–77. <https://doi.org/10.5194/se-12-59-2021>
- Bott, M. (1959). The mechanics of oblique slip faulting. *Geological Magazine*, 96(2), 109–117. <https://doi.org/10.1017/S0016756800059987>
- Brown, A. R. (Ed.) (2011). 1. Introduction. In *Interpretation of Three-Dimensional Seismic Data* (pp. 1–30). Society of Exploration Geophysicists and American Association of Petroleum Geologists. <https://doi.org/10.1190/1.9781560802884.ch1>
- Cameron, T. D. J. (1993). Triassic, Permian and pre-Permian of the Central and Northern North Sea. In K. RWO'B & W. G. Cordey (Eds.), *Lithostratigraphic Nomenclature of the UK North Sea 4* (p. 163). BGS, HMSO [4, 7, 8].
- Cardozo, N., & Allmendinger, R. W. (2013). Spherical projections with OSXStereonet. *Computers & Geosciences*, 51, 193–205. <https://doi.org/10.1016/j.cageo.2012.07.021>
- Carne, R. C., & Little, T. A. (2012). Geometry and scale of fault segmentation and deformational bulging along an active oblique-slip fault (Wairarapa fault, New Zealand). *GSA Bulletin*, 124(7–8), 1365–1381. <https://doi.org/10.1130/B30535.1>
- Chopra, S. (2009). Interpreting fractures through 3D seismic discontinuity attributes and their visualisation. Recorder, CSEG. Number 8.
- Chopra, S., & Marfurt, K. J. (2007). Seismic attributes for fault/fracture characterisation. In *SEG Technical Program Expanded Abstracts* (pp. 1520–1524). <https://doi.org/10.1190/1.2792785>
- Clemmensen, L. B. (1987). Complex star dunes and associated aeolian bedforms, Hopeman Sandstone (Permo-Triassic), Moray Firth Basin, Scotland. In L. Frostick, & I. Reid (Eds.), *Desert Sediments: Ancient and Modern* (Vol. 35, pp. 213–231). Geological Society, London, Special Publications <https://doi.org/10.1144/GSL.SP.1987.035.01.15>
- Coward, M. P., Enfield, M. A., & Fischer, M. W. (1989). Devonian basins of Northern Scotland: extension and inversion related to Late Caledonian - Variscan tectonics. *Geological Society, London, Special Publications*, 44(1), 275–308. <https://doi.org/10.1144/GSL.SP.1989.044.01.16>
- Davies, R. J., Turner, J. D., & Underhill, J. R. (2001). Sequential dip-slip fault movement during rifting: A new model for the evolution of the Jurassic trilete North Sea rift system. *Petroleum Geoscience*, 7(4), 371–388. <https://doi.org/10.1144/petgeo.7.4.371>
- Delvaux, D., Moeys, R., Stapel, G., Petit, C., Levi, K., Miroshnichenko, A., Ruzhich, V., & San'kov, V. (1997). Paleostress reconstructions and geodynamics of the Baikal region, Central Asia, Part 2. Cenozoic rifting. *Tectonophysics*, 282(1–4), 1–38. [https://doi.org/10.1016/S0040-1951\(97\)00210-2](https://doi.org/10.1016/S0040-1951(97)00210-2)
- Deng, H., & McClay, K. (2021). Three-dimensional geometry and growth of a basement-involved fault network developed during multiphase extension, Enderby Terrace, North West Shelf of Australia. *GSA Bulletin*, 133(9–10), 2051–2078. <https://doi.org/10.1130/B35779.1>
- Deng, H., McClay, K., & Bilal, A. (2020). 3D structure and evolution of an extensional fault network of the eastern Dampier Sub-basin, North West Shelf of Australia. *Journal of Structural Geology*, 132, 103972. <https://doi.org/10.1016/j.jsg.2019.103972>
- Deng, H., McClay, K., & Bilal, A. (2021). Multiphase activation of the boundary fault system of the eastern Dampier subbasin, Northwest Shelf of Australia. *AAPG Bulletin*, 105(1), 157–188. <https://doi.org/10.1306/03022019160>
- Di, H., & Gao, D. (2017). Seismic attribute-aided fault detection in petroleum industry: A review. In D. Martion (Ed.), *Fault detection: Methods, Applications and Technology* (pp. 53–80). Nova Science Publishers.
- Edwards, H. E., Becker, A. D., & Howell, J. A. (1993). Compartmentalisation of an aeolian sandstone by structural heterogeneities: Permo-Triassic Hopeman Sandstone, Moray Firth, Scotland. In C. P. North, & D. J. Prosser (Eds.), *Characterisation of Fluvial and Aeolian Reservoirs* (Vol. 73, pp. 339–365). Geological Society, London, Special Publications. <https://doi.org/10.1144/GSL>
- Farrell, N. J. C., Healy, D., & Taylor, C. W. (2014). Anisotropy of permeability in faulted porous sandstones. *Journal of Structural Geology*, 63, 50–67. <https://doi.org/10.1016/j.jsg.2014.02.008>
- Fazlikhani, H., Aagotnes, S. S., Refvem, M. A., Wright, J. H., Bell, R. E., Fossen, H., Gawthorpe, R. L., Jackson, C.-A.-L., & Rotevatn, A. (2020). Strain migration during multiphase extension, Stord Basin, northern North Sea rift. *Basin Research*, 33, 1474–1496. <https://doi.org/10.1111/bre.12522>
- Fossen, H., Schultz, R. A., Shipton, Z. K., & Mair, K. (2007). Deformation bands in sandstone: A review. *Journal of the Geological Society*, 164(4), 755–769. <https://doi.org/10.1144/0016-76492006-036>
- Fournier, M., Bellahsen, N., Fabbri, O., & Gunnell, Y. (2004). Oblique rifting and segmentation of the NE Gulf of Aden passive margin.

- Geochemistry, Geophysics, Geosystems*, 5, Q11005. <https://doi.org/10.1029/2004GC000731>
- Frostick, L., Reid, I., Jarvis, J., & Eardley, H. (1988). Triassic sediments of the Inner Moray Firth, Scotland: Early rift deposits. *Journal of the Geological Society*, 145(2), 235–248.
- Giba, M., Walsh, J. J., & Nicol, A. (2012). Segmentation and growth of an obliquely reactivated normal fault. *Journal of Structural Geology*, 39, 253–267. <https://doi.org/10.1016/j.jsg.2012.01.004>
- Glennie, K. W., Higham, J., & Stemmerik, L. (2003). Permian. In D. Evans, & C. Graham (Eds.), *The Millennium Atlas: Petroleum Geology of the Central and Northern North Sea* (pp. 91–103). Geological Society.
- Glennie, K., & Hurst, A. (2007). Fluidization and associated soft-sediment deformation in eolian sandstones: Hopeman Sandstone (Permian), Scotland, and Rotliegend, North Sea. In A. Hurst, & J. Cartwright (Eds.), *Sand Injectites: Implications for Hydrocarbon Exploration and Production* (Vol. 87, pp. 245–252). AAPG Memoir.
- Goldsmith, P. J., Hudson, G., & van Veen, P. (2003). Triassic. In D. Evans, C. Graham, A. Armour, & P. Bathurst (Eds. and coordinators), *The Millennium Atlas: Petroleum Geology of the Central and Northern North Sea* (pp. 105–128). The geological society of London.
- Hansen, J.-A., Bergh, S. G., & Henningsen, T. (2012). Mesozoic rifting and basin evolution on the Lofoten and Vesterålen Margin, North-Norway; Time constraints and regional implications. *Norwegian Journal of Geology*, 91, 203–228. <https://doi.org/10.1111/bre.12358>
- Henstra, G. A., Berg Kristensen, T., Rotevatn, A., & Gawthorpe, R. L. (2019). How do pre-existing normal faults influence rift geometry? A comparison of adjacent basins with contrasting underlying structure on the Lofoten Margin, Norway. *Basin Research*, 31(6), 1083–1097. <https://doi.org/10.1111/bre.12358>
- Johnstone, G. S., & Mykura, W. (1989). *British Regional Geology: The Northern Highlands of Scotland* (Vol. 2). HM Stationery Office.
- Kamb, W. B. (1959). Ice petrofabric observations from Blue Glacier, Washington, in relation to theory and experiment. *Journal of Geophysical Research*, 64(11), 1891–1909. <https://doi.org/10.1029/JZ064i011p01891>
- Koson, S., Chenrai, P., & Choowong, M. (2014). Seismic attributes and their applications in seismic geomorphology. *Bulletin of Earth Sciences of Thailand*, 6(1), 1–9.
- Lăpădat, A., Imber, J., Yielding, G., Iacopini, D., McCaffrey, K. J. W., Long, J. J., & Jones, R. R. (2016). Occurrence and development of folding related to normal faulting within a mechanically heterogeneous sedimentary sequence: A case study from Inner Moray Firth, UK. *Geological Society, London, Special Publications*, 439, 373–394. <https://doi.org/10.1144/SP439.18>
- Le Breton, E., Cobbold, P. R., & Zanella, A. (2013). Cenozoic reactivation of the Great Glen Fault, Scotland: Additional evidence and possible causes. *Journal of the Geological Society*, 170(3), 403–415.
- Linsley, P. N., Potter, H. C., McNab, G., & Racher, D. (1980). The Beatrice field, Inner Moray Firth, U.K. North Sea. In M. T. Halbouty (Ed.), *Giant Oil and Gas Fields of the Decade 1968-1978* (Vol. 30, pp. 117–129). Memoir of the American Association of Petroleum Geologists.
- Long, J. J., & Imber, J. (2010). Geometrically coherent continuous deformation in the volume surrounding a seismically imaged normal fault-array. *Journal of Structural Geology*, 32, 222–234. <https://doi.org/10.1016/j.jsg.2009.11.009>
- Lovecchio, J. P., Rohais, S., Joseph, P., Bolatti, N. D., Kress, P. R., Gerster, R., & Ramos, V. A. (2018). Multistage rifting evolution of the Colorado basin (offshore Argentina): Evidence for extensional settings prior to the South Atlantic opening. *Terra Nova*, 30, 359–368. <https://doi.org/10.1111/ter.12351>
- Macgregor, D. (2015). History of the development of the East African Rift System: A series of interpreted maps through time. *Journal of African Earth Sciences*, 101, 232–252. <https://doi.org/10.1016/j.jafrearsci.2014.09.016>
- Maithel, S. A., Garner, P. A., & Whitmore, J. H. (2015). Preliminary assessment of the petrology of the Hopeman Sandstone (Permo-Triassic), Moray Firth Basin, Scotland. *Scottish Journal of Geology*, 51(2), 177–184. <https://doi.org/10.1144/sjg2014-028>
- McQuillin, R., Donato, J. A., & Tulstrup, J. (1982). Development of basins in the Inner Moray Firth and the North Sea by crustal extension and dextral displacement of the Great Glen Fault. *Earth and Planetary Science Letters*, 60(1), 127–139.
- Michael, A. J. (1984). Determination of stress from slip data: Faults and folds. *Journal of Geophysical Research: Solid Earth* (1978–2012), 89(B13), 11517–11526.
- Morley, C. K. (2016). The impact of multiple extension events, stress rotation and inherited fabrics on normal fault geometries and evolution in the Cenozoic rift basins of Thailand. In C. Childs, R. E. Holdsworth, C.-A.-L. Jackson, T. Manzocchi, J. J. Walsh, & G. Yielding (Eds.), *The Geometry and Growth of Normal Faults* (Vol. 439). Geological Society, London, Special Publications. <https://doi.org/10.1144/SP439.3>
- Mostafa, M. E. (2005). Iterative direct inversion: An exact complementary solution for inverting fault-slip data to obtain palaeostresses. *Computers & Geosciences*, 31, 1059. <https://doi.org/10.1016/j.cageo.2005.02.012>
- Naylor, H., Turner, P., Vaughan, D. J., & Fallick, A. E. (1989). The Cherty Rock, Elgin: A petrographic and isotopic study of a Permo-Triassic calccrete. *Geological Journal*, 24, 205–221. <https://doi.org/10.1002/gj.3350240305>
- Peacock, J. D., Berridge, N. G., Harris, A. L., & May, F. (1968). Geology of the Elgin District. In *Memoirs of the Geological Survey* (p. 54e77). H.M.S.O.
- Petrel. (2021). Petrel Guru software support for background theory.
- Pigott, J. D., Kang, M. H., & Han, H. C. (2013). First order seismic attributes for clastic seismic facies interpretation: Examples from the East China Sea. *Journal of Asian Earth Sciences*, 66, 34–54. <https://doi.org/10.1016/j.jseae.2012.11.043>
- Quinn, O. F. (2005). *Fault Controlled Fluid Flow and Quartz Cementation in Porous Sandstones* [Unpublished PhD thesis]. University of Edinburgh.
- Ragon, T., Nutz, A., Schuster, M., Ghienne, J. F., Ruffet, G., & Rubino, J. L. (2018). Evolution of the northern Turkana Depression (East African Rift System, Kenya) during the Cenozoic rifting: New insights from the Ekitale Basin (28–25.5Ma). *Geological Journal*, 54, 3468–3488. <https://doi.org/10.1002/gj.3339>
- Rawson, P., & Riley, L. A. (1982). Latest Jurassic-Early Cretaceous events and the late Cimmerian unconformity in North Sea area. *AAPG Bulletin*, 66, 2628–2648. <https://doi.org/10.1306/03B5AC87-16D1-11D7-8645000102C1865D>
- Roberts, A. M., Badley, M. E., Price, J. D., & Huck, I. W. (1990). The structural history of a transtensional basin: Inner Moray Firth, NE Scotland. *Journal of the Geological Society*, 147(1), 87–103.

- Roberts, A. M., Price, J. D., & Badley, M. E. (1989). Discussion on Triassic sediments of the Inner Moray Firth, Scotland: Early rift deposits. *Journal of the Geological Society*, *146*, 361–363. <https://doi.org/10.1144/gsjgs.146.2.0361>
- Rotevatn, A., Fossmark, H. S. S., Bastesen, E., Thorsheim, E., & Torabi, A. (2016). Do deformation bands matter for flow? Insights from permeability measurements and flow simulations in porous carbonate rocks. *Petroleum Geoscience*, *23*, 104–119. <https://doi.org/10.1144/petgeo2016-038>
- Rotevatn, A., Kristensen, T. B., Ksienzyk, A. K., Wemmer, K., Henstra, G. A., Midtkandal, I., Grundvåg, S.-A., & Andresen, A. (2018). Structural inheritance and rapid rift-length establishment in a multiphase rift: The East Greenland rift system and its Caledonian orogenic ancestry. *Tectonics*, *37*, 1858–1875. <https://doi.org/10.1029/2018TC005018>
- Rotevatn, A., Sandve, T. H., Keilegavlen, E., Kolyukhin, D., & Fossen, H. (2013). Fossen Deformation bands and their impact on fluid flow in sandstone reservoirs: the role of natural thickness variations. *Geofluids*, *13*, 359–371. <https://doi.org/10.1111/gfl.12030>
- Sasvári, Á., & Baharev, A. (2014). SG2PS (structural geology to post script converter) – A graphical solution for brittle structural data evaluation and paleostress calculation. *Computers & Geosciences*, *66*, 81–93.
- Seranne, M. (1992). Devonian extensional tectonics versus Carboniferous inversion in the northern Orcadian basin. *Journal of the Geological Society*, *149*(1), 27–37. <https://doi.org/10.1144/gsjgs.149.1.0027>
- Shipton, Z. K., Evans, J. P., Robeson, K. R., Forster, C. B., & Snelgrove, S. (2002). Structural heterogeneity and permeability in faulted eolian sandstone: Implications for subsurface modeling of faults. *AAPG Bulletin*, *86*(5), 863–883.
- Spang, J. (1972). Numerical method for dynamic analysis of calcite twin lamellae. *Geological Society of America Bulletin*, *84*, 134–150. [https://doi.org/10.1130/0016-7606\(1972\)83\[467:NMFDAO\]2.0.CO;2](https://doi.org/10.1130/0016-7606(1972)83[467:NMFDAO]2.0.CO;2)
- Steel, R., & Ryseth, A. (1990). The Triassic — Early Jurassic succession in the northern North Sea: Megasequence stratigraphy and intra-Triassic tectonics. *Geological Society, London, Special Publications*, *55*, 139–168. <https://doi.org/10.1144/GSL.SP.1990.055.01.07>
- Stephenson, D., & Gould, D. (1995). The Grampian Highlands, 4th ed. British Regional Geology Series, x 261 pp. London: HMSO for the British Geological Survey. ISBN 0 11 884521 7. *Geological Magazine*, *133*(4), 506. <https://doi.org/10.1017/S0016756800007779>
- Tamas, A., Holdsworth, R. E., Underhill, J. R., Tamas, D. M., Dempsey, E. D., Hardman, K., Bird, A., McCarthy, D., McCaffrey, K. J. W., & Selby, D. (2021). New onshore insights into the role of structural inheritance during Mesozoic opening of the Inner Moray Firth Basin, Scotland. *Journal of the Geological Society*, *179*(2), jgs2021-066. <https://doi.org/10.1144/jgs2021-066>
- Thomson, K. (1993). *Tertiary Tectonics and Uplift of the Inner Moray Firth and Adjacent Areas* [PhD thesis]. University of Edinburgh.
- Thomson, K., & Hillis, R. R. (1995). Tertiary structuration and erosion of the Inner Moray Firth. In R. A. Scrutton, M. S. Stoker, G. B. Shimmield, & A. W. Tudhope (Eds.), *The Tectonics, Sedimentation and Palaeoceanography of the North Atlantic Region* (Vol. 90, pp. 249–269). Geological Society, London, Special Publications.
- Thomson, K., & Underhill, J. R. (1993). Controls on the development and evolution of structural styles in the Inner Moray Firth Basin. In *Petroleum Geology of Northwest Europe: Proceedings of the 4th Conference on Petroleum Geology of NW Europe* (pp. 1167–1178). Europe, London.
- Tomasso, M., Underhill, J. R., Hodgkinson, R. A., & Young, M. J. (2008). Structural styles and depositional architecture in the Triassic of the Ninian and Alwyn North fields: Implications for basin development and prospectivity in the Northern North Sea. *Marine and Petroleum Geology*, *25*, 588–605. <https://doi.org/10.1016/j.marpetgeo.2007.11.007>
- Trewin, N., & Hurst, A. (2009). Excursion Guide to the Geology of East Sutherland and Caithness, 2nd ed. Aberdeen Geological Society and Dunedin Press. *Geological Magazine*, *147*(5), 798–799.
- Underhill, J. R. (1991). Implications of Mesozoic - Recent basin development in the western Inner Moray Firth, UK. *Marine and Petroleum Geology*, *8*, 359–369.
- Underhill, J. R., & Brodie, J. A. (1993). Structural geology of Easter Ross, Scotland: Implications for movement on the Great Glen fault zone. *Journal of the Geological Society*, *150*(3), 515–527.
- Underhill, J. R., & Woodcock, N. H. (1987). Faulting mechanisms in high-porosity sandstones; New Red Sandstone, Arran, Scotland. In M. E. Jones, & R. M. F. Preston (Eds.), *Deformation of Sediments and Sedimentary Rocks* (Vol. 29, pp. 91–105). Geological Society Special Publication.
- Walker, A. D. (1973). The age of the Cuttie's Hillock sandstone (Permo-Triassic) of the Elgin area. *Scottish Journal of Geology*, *9*, 177–183. <https://doi.org/10.1144/sjg09030177>
- Wallace, R. E. (1951). Geometry of shearing stress and relation to faulting. *The Journal of Geology*, *59*(2), 118–130.
- Wilson, R. W., Holdsworth, R. E., Wild, L. E., McCaffrey, K. J. W., England, R. W., Imber, J., & Strachan, R. A. (2010). Basement influenced rifting and basin development: a reappraisal of post-Caledonian faulting patterns from the North Coast Transfer Zone, Scotland. *Geological Society, London, Special Publications*, *335*, 795–826.

SUPPORTING INFORMATION

Additional supporting information may be found in the online version of the article at the publisher's website.

How to cite this article: Tamas, A., Holdsworth, R. E., Underhill, J. R., Tamas, D. M., Dempsey, E. D., McCarthy, D. J., McCaffrey, K. J. W., & Selby, D. (2022). Correlating deformation events onshore and offshore in superimposed rift basins: The Lossiemouth Fault Zone, Inner Moray Firth Basin, Scotland. *Basin Research*, *34*, 1314–1340. <https://doi.org/10.1111/bre.12661>